White Rose Research Online

eprints@whiterose.ac.uk
https://eprints.whiterose.ac.uk
Universities of Leeds, Sheffield and York

Deposited via The University of Leeds.

White Rose Research Online URL for this paper:
https://eprints.whiterose.ac.uk/id/eprint/245777/

Version: Accepted Version

Article:
Nagegowda, K., Mahabaleshwar, U.S., Manca, O. et al. (Accepted: 2026) An effect of Boussinesq-Stokes suspensions fluid with CNTs and heat transfer: An unsteady case. Heat Transfer. ISSN: 2688-4534 (In Press)

This is an author produced version of an article accepted for publication in Heat Transfer, made available via the University of Leeds Research Outputs Policy under the terms of the Creative Commons Attribution License (CC-BY), which permits unrestricted use, distribution and reproduction in any medium, provided the original work is properly cited.

Reuse
This article is distributed under the terms of the Creative Commons Attribution (CC BY) licence. This licence allows you to distribute, remix, tweak, and build upon the work, even commercially, as long as you credit the authors for the original work. More information and the full terms of the licence here: https://creativecommons.org/licenses/

Takedown
If you consider content in White Rose Research Online to be in breach of UK law, please notify us by emailing eprints@whiterose.ac.uk including the URL of the record and the reason for the withdrawal request.

UNIVERSITY OF LEEDS
University of Sheffield
UNIVERSITY of York

An effect of Boussinesq-Stokes suspensions fluid with CNTs and heat transfer: An unsteady case

K Nagegowda[1], U S Mahabaleshwar[1*], O Manca[2,] B Buonomo[2], Sergio Nardini[3] Greg de Boer[4]

[1]Department of Studies in Mathematics, Shivagangotri, Davangere University, Davangere-577 007, INDIA, E-mail: nagegowda.k04@gmail.com, u.s.m@davangereuniversity.ac.in,

[2,3]Dipartimento di Ingegneria, Università degli Studi della Campania Luigi Vanvitelli, Aversa, CE, ITALY, Email: oronzio.manca@unicampania.it, bernardo.buonomo@unicampania.it, sergio.nardini@unicampania.it

[4]Institute of Thermofluids (iTF) School of Mechanical Engineering, University of Leeds Woodhouse Lane, Leeds, LS2 9JT, UK. E-mail: G.N.deBoer@leeds.ac.uk

Abstract

Carbon nanotubes are widely used in nanofluids, electronics, and biomedical engineering due to their excellent thermal, electrical, and mechanical capabilities. They are used as an essential for the development of cutting-edge material, energy, and sensing technology. This study aims to investigate the unsteady flow of a non-Newtonian fluid over a permeable extended surface at a stagnation point. Thermal radiation and convective boundary conditions while analyzing heat transfer capabilities. The nonlinear PDE model is converted into nonlinear ODE model via suitable similarity approach and then solved analytically. The analytical solution is for velocity and temperature for several parameters are discussed via graphs. The results reveal that rise in mass transpiration and porosity leads to drop in velocity profile. Also, augmentation in Biot number and solid volume fraction boosts temperature profile.

Keywords: Stretching/shrinking surface, CNT, Couple stress, Thermal radiation, Stagnation point,

1. Introduction:

A Newtonian fluid's flow depiction and real challenges are crucial. The researchers looked at the stretching sheet issue by seeing how it improved a number of applications in the domains of engineering, high-temperature processes, physics, polymer processing, and space technology. In the field of Newtonian fluids, heat transport is essential, and knowledge of rheological properties is crucial for technological applications. Stretching sheets have been researched by several researchers. Sakiadis [1] The initial study focused on a thick boundary layer flow, a persistent surface with a constant impact rate. Crane [2], extending the Sakiadis problem to an elongated sheet, yields an exact solution. Hayat *et al* [3] explored an

axisymmetric flow of third-grade fluid with a stretching cylinder. It was discovered that as the shear thinning/thickening parameter and magnetic parameter increase, the velocity profile diminishes. Mohanty *et al.* [4] used interfacial nanolayers to analyze the thermal and irreversibility of an unsteady hybrid nanofluid flow over a spinning sphere with C-C heat flux model. It was discovered that axial velocity rises with the rotational parameter.

Mahabaleshwar *et al*. [5] studied the hybrid nanofluid flow with radiation and suction/injection across a shrinking/stretching surface, the study's outcomes enhancing the thermal radiation, increasing the temperature profile.

CNTs have a six-fold greater heat capacity than conventional materials at typical temperatures. Carbon nanotubes (CNTs) have a cylindrical nanostructure. Carbon nanotubes may be classified as SWCNTs and MWCNTs. In order to analyze irreversibility of drug administration, Kumar *et al.* [6] investigated the influence of activation energy on blood based micropolar nanofluid flow through a permeable squeezing channel. From the result, it has been demonstrated that SWCNTs are superior to MWCNTs in terms of increasing the system's velocity, temperature, and irreversibility. Sahu *et al*. [7] studied the thermal interference and Darcy-Forchheimer flow behaviour with SWCNT/MWCNT suspensions as a result of shrinking rotating disk; the study reveals that with the inclusion of a significant interfacial nanolayer, the heat transfer rate upgrades. Iijima [8] studied the Helical microtubules of graphitic carbon, result outcomes It has been demonstrated that SWCNTs are more successful and efficient than MWCNTs at increasing the system's velocity, temperature, and irreversibility. Considering chemical reaction and non-linear radiation, Kumar *et al.* [9] studied irreversibility phenomenon of 3D flow of Carbon nanotubes. The research shows that drag force and rate of heat transfer is greater in SWCNT compared to MWCNT fluid flow.

Thermal radiation is the transport of heat by electromagnetic waves released by all substances at a certain temperature. In contrast to conduction and convection, it propagates without the use of a medium. Thermal radiation is important for managing heat transfer rates in high-temperature flows, such as those found in aerospace, power production, and nanofluid systems. The rate of heat and mass transfer of boundary layer flow across a couple stress fluid in the presence of MHD was explored by Mahabaleshwar *et al.* [10]. Yedhri *et al.* [11] scrutinized the impact of radiation, hall current, joule heating on unsteady convective flow across a Perpendicular plate. A computational model of a rotating flow of Carbon nanotube under the impact of ohmic heating radiation, and chemical conversion was investigated by Eswaramoorthi *et al.* [12]. As a result, heat transfer properties boosted for rising values of radiation and temperature difference parameters. Divya *et al.* [14] conducted numerical

analysis on non-Newtonian hybrid nanofluid flow under the influence of radiation with regression model. According to study, rise in temperature profile was found for larger values of radiation.

By taking into account the impact of tiny rotations and size-dependent stresses in the fluid, the couple stress fluid theory expands on the traditional Newtonian model. It takes into consideration the existence of pair stresses brought on by fluid particle rotation. For fluids that include suspended particles or microstructures, this hypothesis is important. It helps research microfluidic systems, blood flow, and lubrication. The model contributes to a more realistic description of non-Newtonian behaviour in complicated fluids. Mahabaleshwar *et al.* [14] explored an MHD couple stress fluid produced by a perforated sheet undergoing linear stretching with heat transfer. Result outcomes conduction heat transmission is preferred, and the temperature of the fluid bulk rises as the value of the couple stress grows, much like the Chandrashekar number. On applying Fourier and Fick's law, Dolat *et al.* [15] examined a Casson MHD tetra hybrid nanofluid flow across a parallel surface under the effects of Couple stress and porous medium. The results reveal that as couple stress intensifies, reduction in all velocity, temperature, and concentration profiles is observed. The impact of hall current Lorentz force, and nonlinear thermal radiation on Couple stress fluid over Riga plate was studied by Rana *et al.* [16]. The research discovered that growing values of couple stress parameter rises temperature distribution within boundary layer. Kumar and Jangili [17] explored flow and heat transfer capabilities of couple stress fluid under the influence of electromagnetic field. Kumar and Nandkeolyar [18] studied MHD non-Newtonian fluid flow through a channel in the presence of nonlinear thermal radiation.

Flows across bodies like cylinders, spheres, and stretched sheets frequently exhibit stagnation spots. Aerodynamics, heat transmission, and engineering design all depend on the understanding of stagnation point flow. It facilitates comprehension of surface pressure distribution and boundary layer behaviour. Reddy *et al.* [19] studied the Williamson hybrid nanofluid magnetohydrodynamic stagnation point flow by stretching sheet in a porous medium with a chemical reaction and heat source. The results indicate that the velocity field declines with growth in the magnetic field and the porosity parameter for both hybrid and mono nanofluid. Singh *et al.* [20] discovered that the Stagnation point flow of hybrid nanofluid driven towards a sinusoidal-radius permeable circular cylinder results in observed enhanced stagnation parameter increases velocity. Karthik and Vinaykumar [21] estimated the impact of solar radiation on EMHD dusty hybrid nanofluid at stagnation point across a permeable

stretched sheet. Vishwanath *et al.* [22] studied the impact of viscous dissipation and heat source on micropolar nanofluid using spectral and Haar wavelet collocation.

The original aspect of this study is its investigation of the impact of unsteady CNT fluid flow at stagnation point of a Boussinesq-stokes suspension fluid across a stretched sheet. Using the proper similarity transformations, the governing coupled nonlinear equations are converted to a system of ordinary differential equations. The energy equation is solved analytically and expressed the incomplete gamma function. The solution is discussed both in upper and lower branches indicating dual solution.

2. Mathematical formulation and solution

The present study incorporates unsteady, incompressible flow across an extending/shrinking surface. The nanofluid comprises of CNTs which enhances the thermophysical characteristics of nanofluid flow. The flow's free stream velocity is expressed as $U_\infty = U_0 x/1-\gamma t$ and the wall stream velocity at the wall is calculated using $U_w = \lambda U_0 x/1-\gamma t$ where U_0 denotes constant velocity, λ denotes shrinking/stretching parameter, and t represents time. Assuming that the average absorption rates and wall motion speed are represented by U_w and V_w. (T, T_∞) indicates the temperature of the fluid at the surface and at the far field. The governing equations for this study are as follows [23-26]:

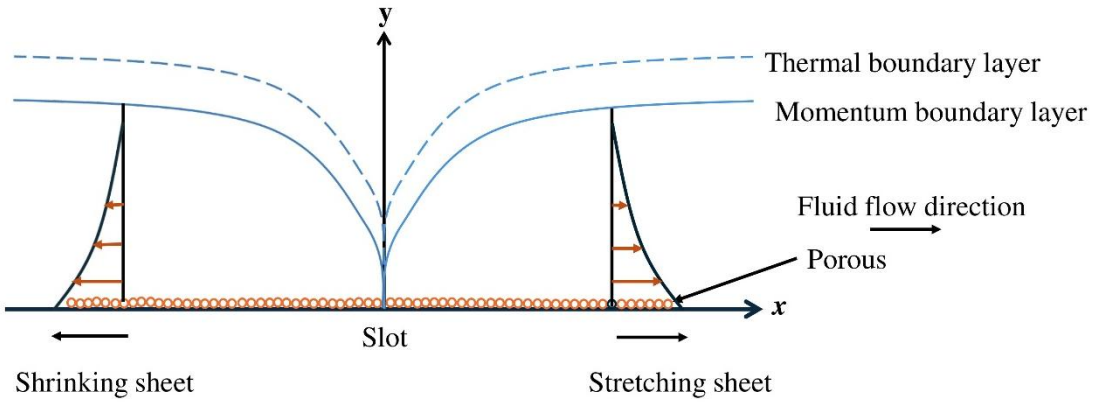


Fig. 1: Schematic diagram for stretching/shrinking boundary.

$$\frac{\partial v}{\partial y} + \frac{\partial u}{\partial x} = 0\,, \tag{1}$$

$$\rho_{nf}\left(u\frac{\partial u}{\partial x}+v\frac{\partial u}{\partial y}+\frac{\partial u}{\partial t}\right)+\eta_0\left(\frac{\partial^4 u}{\partial y^4}\right)=\rho_{nf}\left(\frac{\partial U_\infty}{\partial t}+U_\infty\frac{\partial U_\infty}{\partial x}\right)+\mu_{nf}\left(\frac{\partial^2 u}{\partial y^2}+\frac{\partial^2 u}{\partial x^2}\right)-\frac{\mu_{nf}}{K}\left(u-U_\infty\right) \tag{2}$$

$$\rho_{nf}\left(u\frac{\partial v}{\partial x}+v\frac{\partial v}{\partial y}+\frac{\partial v}{\partial t}\right)=\mu_{nf}\left(\frac{\partial^2 v}{\partial x^2}+\frac{\partial^2 v}{\partial y^2}\right)-\frac{\partial P}{\partial y}, \tag{3}$$

$$\left(\frac{\partial T}{\partial t}+u\frac{\partial T}{\partial x}+v\frac{\partial T}{\partial y}\right)=\frac{\kappa_{nf}}{\left(\rho Cp\right)_{nf}}\left(\frac{\partial^2 T}{\partial y^2}+\frac{\partial^2 T}{\partial x^2}\right)-\frac{1}{\left(\rho Cp\right)_{nf}}\frac{\partial q_r}{\partial y}. \tag{4}$$

The boundary conditions are given by [27]:

$$u=U_w,\ v=\sqrt{\frac{U_0\upsilon_f}{1-\gamma t}}V_w,\ -\kappa_{nf}\frac{\partial T}{\partial y}=h_f\left(T_f-T\right)\qquad \text{at } y=0,$$

$$u\to 0,\ \frac{\partial u}{\partial y}\to 0,\ \frac{\partial^2 u}{\partial y^2}\to\infty,\ T\to T_\infty,\qquad \text{as } y\to\infty. \tag{5}$$

The pressure term is given as follows:

$$-\frac{1}{\rho}\frac{\partial P}{\partial x}=\left(1-\beta\right)\frac{\varepsilon_2 U_0^2 x}{\left(1-\gamma t\right)^2}, \tag{6}$$

The suitable similarity transformation for the present flow problem is:

$$\left.\begin{aligned}&\eta=y\sqrt{\frac{U_0}{\upsilon_f\left(1-\gamma t\right)}},\ \left(1-\gamma t\right)u=U_0 x f_\eta\left(\eta\right),\\&\left(1-\gamma t\right)^{1/2}v=-\left(\upsilon_f U_0\right)^{1/2}f\left(\eta\right),\theta\left(\eta\right)\left(T_w-T_\infty\right)=T-T_\infty.\end{aligned}\right\}, \tag{7}$$

On employing the similarity parameters 7, eqn. 1-4 reduced to:

$$\Lambda f_{\eta\eta\eta\eta\eta}\left(\eta\right)-\frac{\varepsilon_1}{\varepsilon_2}f_{\eta\eta\eta}\left(\eta\right)-\left(\beta\left\{f_\eta\left(\eta\right)+\frac{\eta}{2}f_{\eta\eta}\left(\eta\right)-1\right\}+f\left(\eta\right)f_{\eta\eta}\left(\eta\right)+1\right)-\Gamma\left(1-f_\eta\left(\eta\right)\right)=0$$

,(8)

$$\frac{\left(\varepsilon_4+N_R\right)}{\varepsilon_3\,\mathrm{Pr}}\theta_{\eta\eta}\left(\eta\right)+\left(f\left(\eta\right)-\frac{\beta\eta}{2}\right)\theta_\eta\left(\eta\right)=0. \tag{9}$$

with Bcs,

$$f_\eta\left(0\right)-\lambda=0,\ f\left(0\right)=V_C,\ \theta_\eta\left(0\right)=-Bi\left(1-\theta\left(0\right)\right), \tag{10}$$

$$f_\eta\left(\infty\right)\to 0,\ f_{\eta\eta}\left(\infty\right)\to 0,\ f_{\eta\eta\eta}\left(\infty\right)\to 0,\ \theta\left(\infty\right)\to 0. \tag{11}$$

The various physical parameters are as follows:

$\Lambda = \dfrac{U_0 \eta_0}{(1-\lambda t)\upsilon_f \rho_f}$ - Couple stress parameter $\quad \mathrm{Pr} = \dfrac{\upsilon_f (\rho Cp)_f}{\kappa_f}$ - Prandtl number

$\Gamma = \dfrac{\upsilon_f (1-\gamma t)}{K U_0}$ - Porosity parameter $\quad N_R = \dfrac{16\sigma^* T_\infty^3}{3k^* \kappa_f}$ - Radiation parameter

$\lambda = \dfrac{U_w}{U_0}$ - stretching/shrinking parameter $\quad \beta = \dfrac{\Omega}{U_0}$ - Unsteadiness parameter

$\varepsilon_1 = \dfrac{\mu_{nf}}{\mu_f}$, $\varepsilon_2 = \dfrac{\rho_{nf}}{\rho_f}$, $\varepsilon_3 = \dfrac{(\rho Cp)_{nf}}{(\rho Cp)_f}$,

$\varepsilon_4 = \dfrac{\kappa_{nf}}{\kappa_f}$ - Contants

3. Analytical solution

Condition $F(\eta) = f(\eta) - \eta$ is considered to solve momentum equation, producing equations and boundary conditions are as follows:

$$\Lambda F_{\eta\eta\eta\eta\eta}(\eta) - \frac{\varepsilon_1}{\varepsilon_2} F_{\eta\eta\eta}(\eta) - \eta\left(\frac{\beta}{2}+1\right) F_{\eta\eta}(\eta) - 1 - F_{\eta\eta}(\eta) F(\eta) + (\Gamma - \beta) F_\eta(\eta). \tag{12}$$

and

$$F_\eta(0) = \lambda - 1, \quad F(0) = V_C, \qquad \theta_\eta(0) = Bi\left(1 - \theta(0)\right), \tag{13}$$

$$F_\eta(\infty) \to -1, \quad F_{\eta\eta}(\infty) \to 0, \quad F_{\eta\eta\eta}(\infty) \to 0, \ \theta(\infty) \to 0. \tag{14}$$

3.1. Solution for Velocity

From boundary conditions (13-14), we obtain,

$$F(\eta) = V_C + \lambda \beta^{-1}\left(-e^{-\beta\eta} + 1\right). \tag{15}$$

On applying the assumed solution (15) to (12), the resulting equation is as follows:

$$\Lambda \varepsilon_2 \alpha^4 + (-\varepsilon_2)\alpha - \varepsilon_1 \alpha^2 + \varepsilon_2 V_C \alpha + \varepsilon_2 \Gamma - \frac{\varepsilon_2}{\lambda} = 0. \tag{16}$$

$$\alpha_1 = \frac{1}{2}\sqrt{\left(\frac{2\varepsilon_1}{3\varepsilon_2\Lambda} + A/(3\varepsilon_2\Lambda B) + \frac{1}{3\times 2^{\frac{1}{3}}\varepsilon_2\lambda\Lambda} B\right)} - \frac{1}{2}\sqrt{\left(\frac{4\varepsilon_1}{3\varepsilon_2\Lambda} - A/(3\varepsilon_2\Lambda B) - \frac{1}{3\times 2^{\frac{1}{3}}\varepsilon_2\lambda\Lambda} B - \left(2(-1+V_c)\right)/\left(\Lambda\sqrt{\left(\frac{2\varepsilon_1}{3\varepsilon_2\Lambda} + A\right)/(3\varepsilon_2\Lambda B) + \frac{1}{3\times 2^{\frac{1}{3}}\varepsilon_2\lambda\Lambda} B}\right)\right)}$$

$$\alpha_2 = \frac{1}{2}\sqrt{\left(\begin{array}{l}\frac{2\varepsilon_1}{3\varepsilon_2\Lambda} + A/\left(3\varepsilon_2\Lambda B\right) \\ +\frac{1}{3\times 2^{\frac{1}{3}}\varepsilon_2\lambda\Lambda}B\end{array}\right)} + \frac{1}{2}\sqrt{\left(\begin{array}{l}\frac{4\varepsilon_1}{3\varepsilon_2\Lambda} - A/\left(3\varepsilon_2\Lambda B\right) - \frac{1}{3\times 2^{\frac{1}{3}}\varepsilon_2\lambda\Lambda}B - \left(2\left(-1+V_c\right)\right)/ \\ \left(\Lambda\sqrt{\left(\frac{2\varepsilon_1}{3\varepsilon_2\Lambda}+A\right)/\left(3\varepsilon_2\Lambda B\right)+\frac{1}{3\times 2^{\frac{1}{3}}\varepsilon_2\lambda\Lambda}B}\right)\end{array}\right)}$$

$$\alpha_3 = -\frac{1}{2}\sqrt{\left(\begin{array}{l}\frac{2\varepsilon_1}{3\varepsilon_2\Lambda} + A/\left(3\varepsilon_2\Lambda B\right) \\ +\frac{1}{3\times 2^{\frac{1}{3}}\varepsilon_2\lambda\Lambda}B\end{array}\right)} - \frac{1}{2}\sqrt{\left(\begin{array}{l}\frac{4\varepsilon_1}{3\varepsilon_2\Lambda} - A/\left(3\varepsilon_2\Lambda B\right) - \frac{1}{3\times 2^{\frac{1}{3}}\varepsilon_2\lambda\Lambda}B - \left(2\left(-1+V_c\right)\right)/ \\ \left(\Lambda\sqrt{\left(\frac{2\varepsilon_1}{3\varepsilon_2\Lambda}+A\right)/\left(3\varepsilon_2\Lambda B\right)+\frac{1}{3\times 2^{\frac{1}{3}}\varepsilon_2\lambda\Lambda}B}\right)\end{array}\right)}$$

$$\alpha_4 = -\frac{1}{2}\sqrt{\left(\begin{array}{l}\frac{2\varepsilon_1}{3\varepsilon_2\Lambda} + A/\left(3\varepsilon_2\Lambda B\right) \\ +\frac{1}{3\times 2^{\frac{1}{3}}\varepsilon_2\lambda\Lambda}B\end{array}\right)} + \frac{1}{2}\sqrt{\left(\begin{array}{l}\frac{4\varepsilon_1}{3\varepsilon_2\Lambda} - A/\left(3\varepsilon_2\Lambda B\right) - \frac{1}{3\times 2^{\frac{1}{3}}\varepsilon_2\lambda\Lambda}B - \left(2\left(-1+V_c\right)\right)/ \\ \left(\Lambda\sqrt{\left(\frac{2\varepsilon_1}{3\varepsilon_2\Lambda}+A\right)/\left(3\varepsilon_2\Lambda B\right)+\frac{1}{3\times 2^{\frac{1}{3}}\varepsilon_2\lambda\Lambda}B}\right)\end{array}\right)}$$

where,

$$A = \left(2^{\frac{1}{3}}\left(\varepsilon_1{}^2\lambda - 12\varepsilon_2{}^2\Lambda + 12\varepsilon_2{}^2\Gamma\lambda\Lambda\right)\right),$$

$$B = \left(\begin{array}{l}-2\varepsilon_1{}^3\lambda^3 + 27\varepsilon_2\left(-\varepsilon_2+\varepsilon_2 V_c\right)^2\lambda^3\Lambda + 72\varepsilon_1\varepsilon_2\lambda^2\left(-\varepsilon_2+\varepsilon_2\Gamma\lambda\right)\Lambda \\ +\sqrt{\left(-4\left(\varepsilon_1{}^2\lambda^2 + 12\varepsilon_2\lambda\left(-\varepsilon_2+\varepsilon_2\Gamma\lambda\right)\Lambda\right)^3 + \left(-2\varepsilon_1{}^3\lambda^3 + 27\varepsilon_2\left(-\varepsilon_2+\varepsilon_2 V_c\right)^2\lambda^3\Lambda + 72\varepsilon_1\varepsilon_2\lambda^2\left(-\varepsilon_2+\varepsilon_2\Gamma\lambda\right)\Lambda\right)^2\right)}\end{array}\right)^{\frac{1}{3}}$$

The solution for the velocity profile is $f(\eta) = \eta + V_C + \frac{\lambda\left(1-e^{-\beta\eta}\right)}{\beta}$. (17)

3.2. Solution for Heat Transfer

A new constraint ξ is considered that fulfils the correlation coefficient, which will aid in determining the solution to the heat equation (10) for the stretching/shrinking sheet.

$$\xi = (1-\lambda)\frac{\mathrm{Pr}}{\alpha^2}e^{-\alpha\eta}. \quad (18)$$

With the help of eqn (15) and eqn (18), eqn (9) becomes,

$$\frac{\partial\theta}{\partial\xi}\left(\varepsilon_3\xi+\left(\varepsilon_4+N_R\right)-\varepsilon_3 Pr\left(1+\frac{4\varepsilon_2+\varepsilon_1\Gamma}{\alpha^2}\right)\right)+\xi\frac{\partial^2\theta}{\partial\xi^2}\left(\varepsilon_4+N_R\right)=0. \tag{19}$$

and boundary conditions

$$\frac{Pr}{\alpha}\left(\left(1-\lambda\right)\frac{Pr}{\alpha^2}\right)\left(1-\lambda\right)\theta_\eta=\left(\left(\left(1-\lambda\right)\frac{Pr}{\alpha^2}\right)\theta-1\right)Bi,\ \theta\left(\infty\right)=0. \tag{20}$$

We take $\xi=0$ the singular point is taken and using Frobenius method the solutions of Eq. (19) are analysed using power series approach,

$$\theta\left(\xi\right)=\sum_{r=0}^{\infty}\zeta^{n+r}a_r. \tag{21}$$

Substitute the derived of θ w.r.t ξ which is $\left(\theta_\eta,\theta_{\eta\eta}\right)$ Into eqn. (19), then

$$\begin{aligned}\left(\varepsilon_3\xi+\left(\varepsilon_4+N_R\right)-\varepsilon_3 Pr\left(1+\frac{4}{\alpha^2}\right)\right)\sum_{r=0}^{\infty}\left(n+r\right)a_r\,\xi^{n+r-1}&\\ +\xi\left(\varepsilon_4+N_R\right)\sum_{r=0}^{\infty}\left(n+r-1\right)\left(n+r\right)a_r\,\xi^{n+r-2}&=0\end{aligned} \tag{22}$$

With the reappearance relation to Eq. (22) and $n=0$, $n=1-\frac{k_1}{k_2}$ Individually, we get

$$a_r=-a_{r-1}\frac{\varepsilon_3\left(n+r-1\right)}{\left[k_1+k_2\left(n+r-1\right)\right]\left(r+1\right)}. \tag{23}$$

here, $k_1=\left(\varepsilon_4+N_R\right)-\varepsilon_3\,\mathrm{Pr}\left(\varepsilon_1+\frac{4\varepsilon_2+\varepsilon_1\Gamma}{\alpha^2\varepsilon_2}-\Lambda\alpha^2\right)$,

$k_2=\left(\varepsilon_4+N_R\right)$.

Using recurrence relation, equation (22) is reduced as follows:

$$\theta\left(\xi\right)=C_1C_0+C_2C_0\left(1-\frac{k_1}{k_2}\right)\left(-\varepsilon_3\right)^{-\left(1-\frac{k_1}{k_2}\right)}\left[\Gamma\left(1-\frac{k_1}{k_2},0\right)-\Gamma\left(1-\frac{k_1}{k_2},-\xi\varepsilon_3\right)\right]. \tag{24}$$

where,

$C_1=0$,

$$C_2=\frac{Bi}{\left(-\varepsilon_3\right)^{\frac{k_1}{k_2}-1}c_0\left(1-\frac{k_1}{k_2}\right)}\left\{\exp\left(\left(\lambda-1\right)\varepsilon_3\frac{Pr}{\alpha^2}\right)\alpha\left(-\left(\lambda-1\right)\varepsilon_3\frac{Pr}{\alpha^2}\right)^{1-\frac{k_1}{k_2}}-\right.$$
$$\left.Bi\,\Gamma\left(1-\frac{k_1}{k_2},-\left(\lambda-1\right)\varepsilon_3\frac{Pr}{\alpha^2}\right)+Bi\,\Gamma\left(1-\frac{k_1}{k_2},0\right)\right\}^{-1}. \tag{25}$$

The interpretation of expressions of η is attained by replacing C_1 and C_2 Values in Eqn (24) in terms of the incomplete gamma function are defined as,

$$\theta(\eta)=\frac{\left(1-\frac{k_1}{k_2},0\right)Bi\Gamma-\left(1-\frac{k_1}{k_2},-\frac{Pr}{\alpha^2\left(\varepsilon_4+N_R\right)}e^{-\alpha\eta}\left(\lambda-1\right)\varepsilon_3\right)Bi\Gamma}{\left\{\exp\left(\frac{Pr}{\alpha^2}\left(\lambda-1\right)\varepsilon_3\right)\alpha\left(-\frac{Pr}{\alpha^2}\left(\lambda-1\right)\varepsilon_3\right)^{1-\frac{k_1}{k_2}}+\left(1-\frac{k_1}{k_2},0\right)Bi\Gamma-\left(1-\frac{k_1}{k_2},-\varepsilon_3\frac{Pr}{\alpha^2}\frac{\left(\lambda-1\right)}{\left(\varepsilon_4+N_R\right)}\right)Bi\Gamma\right\}} \quad (26)$$

4. Results and discussion

This section addresses the behaviour of fluid flow velocity and temperature of the fluid flow of couple stress fluid at stagnation point across a stretching/shrinking surface under the influence of couple stress Λ, porosity parameter Γ, λ parameter, V_c and N_R parameter. Similarity transformations are used to convert the controlling PDEs into ODEs. Couple stress and thermal radiation are the causes of this problem. An incomplete gamma function with a Biot number is then used to express the resulting equations. The results are then discussed graphically. The quantitative values of skin friction and Nusselt number obtained in this study, compared with the previous research, are presented in Table 1. The analytical code was validated by comparing it to Hady's previous results for reduced Nusselt number and skin friction coefficient in hybrid nanofluids, including SWCNT and MWCNT. When a hybrid nanofluid mixture of carbon nanotubes (MWCNT, SWCNT) was used instead of a single nanofluid mixture, the quantitative comparisons produced more improved results.

Table 1. Correlation of the quantitative values of $f''(0)$ and $-\theta'(0)$ when $\varepsilon_1=\varepsilon_2=1$ in the absence of Λ and Γ.

Nanoparticles	**Parameters**		**Skin friction** $f_{\eta\eta}(0)$		**Nusselt number** $-\theta_\eta(0)$	
	β	ϕ	Previous study [49]	Present study	Previous study [49]	Present study
MWCNT and SWCNT	1	0.1	1.51280	1.51299	0.40756	0.40789
		0.2	1.45745	1.45751	0.39128	0.39255
	-1	0.1	0.93199	0.93202	1.49102	1.49106
		0.2	0.89790	0.89796	1.32640	1.32648

Fig 2 displays the variation of α with the mass-transpiration parameter V_C for distinct parametric values of the unsteadiness parameter Γ. The curves display two possible solutions, with black dashed lines representing the lower branch and red representing the upper branch. Stronger unsteadiness increases α at a given transpiration value, as seen by the upward and outward movement of the α - V_C Curves on the upper branch. The curves move outward and downward on the lower branch, indicating Γ Once more, but at the unstable solution branch.

Fig 3 shows the relationship between the parameter. α and the mass transpiration parameter V_C for various material parameters Λ Values. The curves show dual solutions, with the higher branch represented by solid red curves and the lower branch represented by dashed black curves. In the upper branch, increasing Λ causes the α -V_C curves to shift upward and outward, suggesting that α Rises for the same mass transpiration value. Lower branch curves move downward and outward, indicating that higher Λ increases the magnitude of α, even in unstable solution regimes.

Figure 4 shows the stretching parameter λ affects α for various Λ values. The curves drop downward as Λ rises, suggesting a larger negative α and increased shear effects in the boundary layer. As Λ increases, the looping structure expands and exhibits more nonlinear flow behaviour. Because of its greater mechanical and thermal strength, the MWCNT nanofluid consistently yields bigger α values than SWCNT. In general, MWCNTs show a larger hydrodynamic response, and Λ greater increases the sensitivity of α to λ.

Figure 5 depicts the impact of Λ constraint on $f_\eta(\eta)$ Profile. Enhancing the couple stress parameter decreases the velocity profile. Physically, this implies that the fluid has a higher internal resistance to shear, slowing the speed of fluid particles near the wall and forcing the velocity to adapt to the free-stream value more rapidly. In microfluidics, lubrication, polymer processing, and biological flows, where microstructural rotations are crucial, this impact is significant.

Fig. 6 displays the effect of the λ on the $f_\eta(\eta)$. The $f_\eta(\eta)$ decreases for reducing values of λ. This is because sheets travel more slowly or compress the fluid when the λ Drops, which lessens the transfer of momentum from the surface to the fluid. The $f_\eta(\eta)$ Decreases as a result of the flow's accelerating driving force becoming weaker. In terms of physical characteristics, it denotes a propensity towards flow separation, a larger boundary layer, and less fluid velocity.

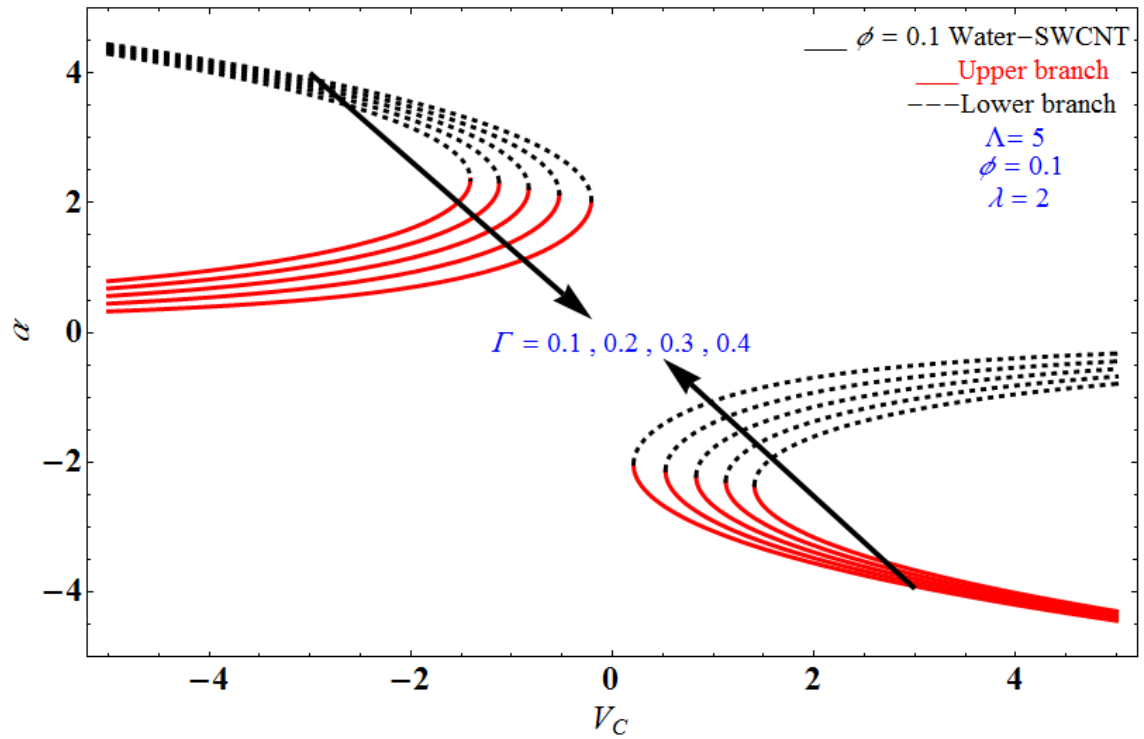


Fig 2. Impact of α verses V_C for distinct values of Γ.

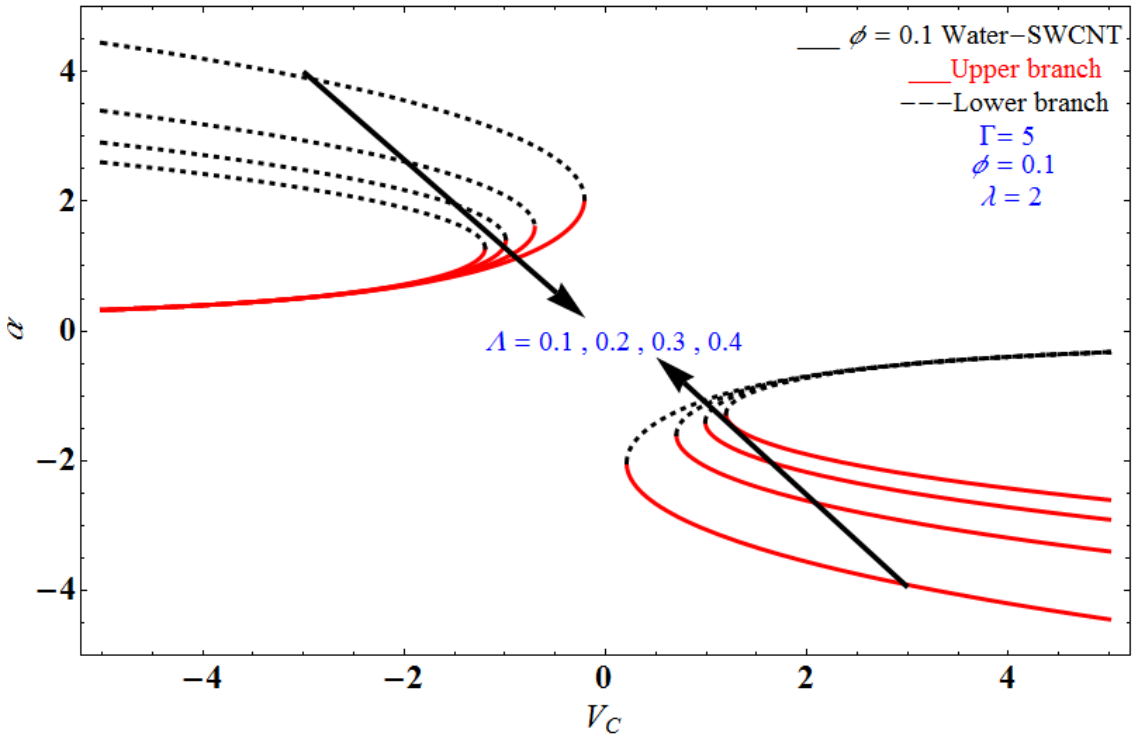


Fig 3. Upshot of α verses V_C for altered values of Λ.

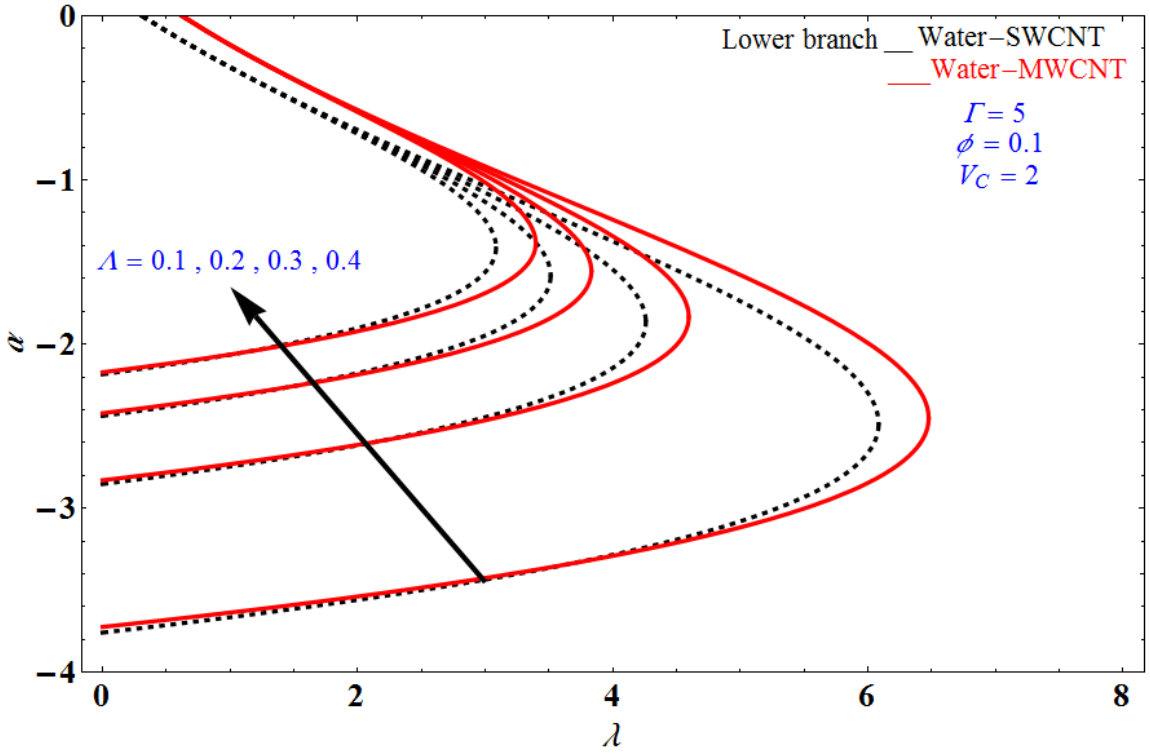


Fig 4. Solution domain α versus λ for various values of Λ.

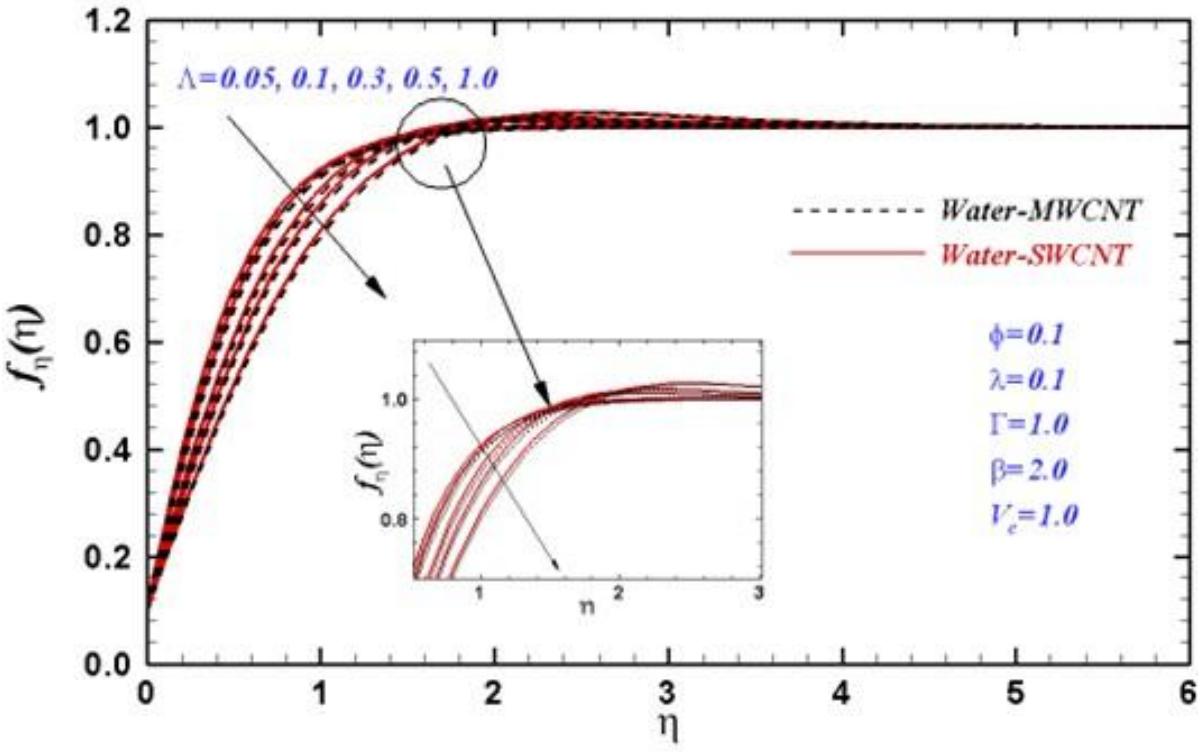


Fig 5. impact of Couple stress constraint Λ on $f_\eta(\eta)$.

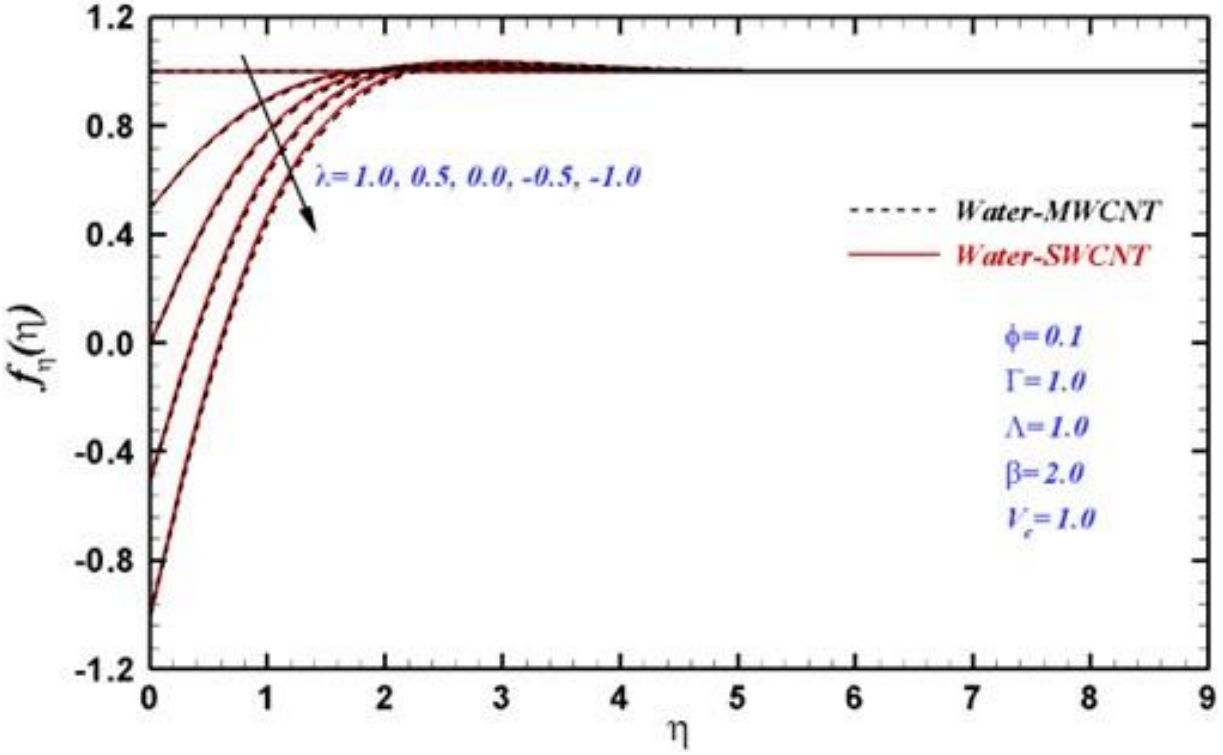


Fig 6. Effect of stretching/shrinking λ on $f_\eta(\eta)$.

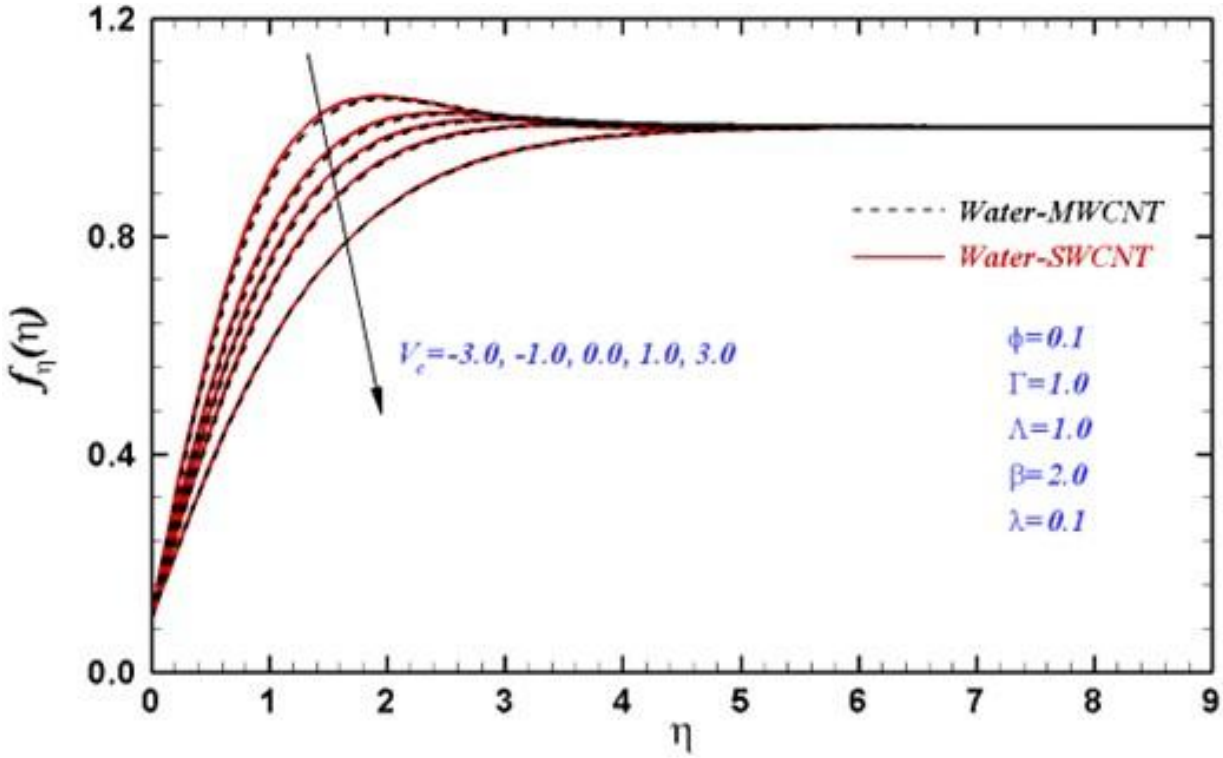


Fig 7. Influence of V_C on $f_\eta(\eta)$.

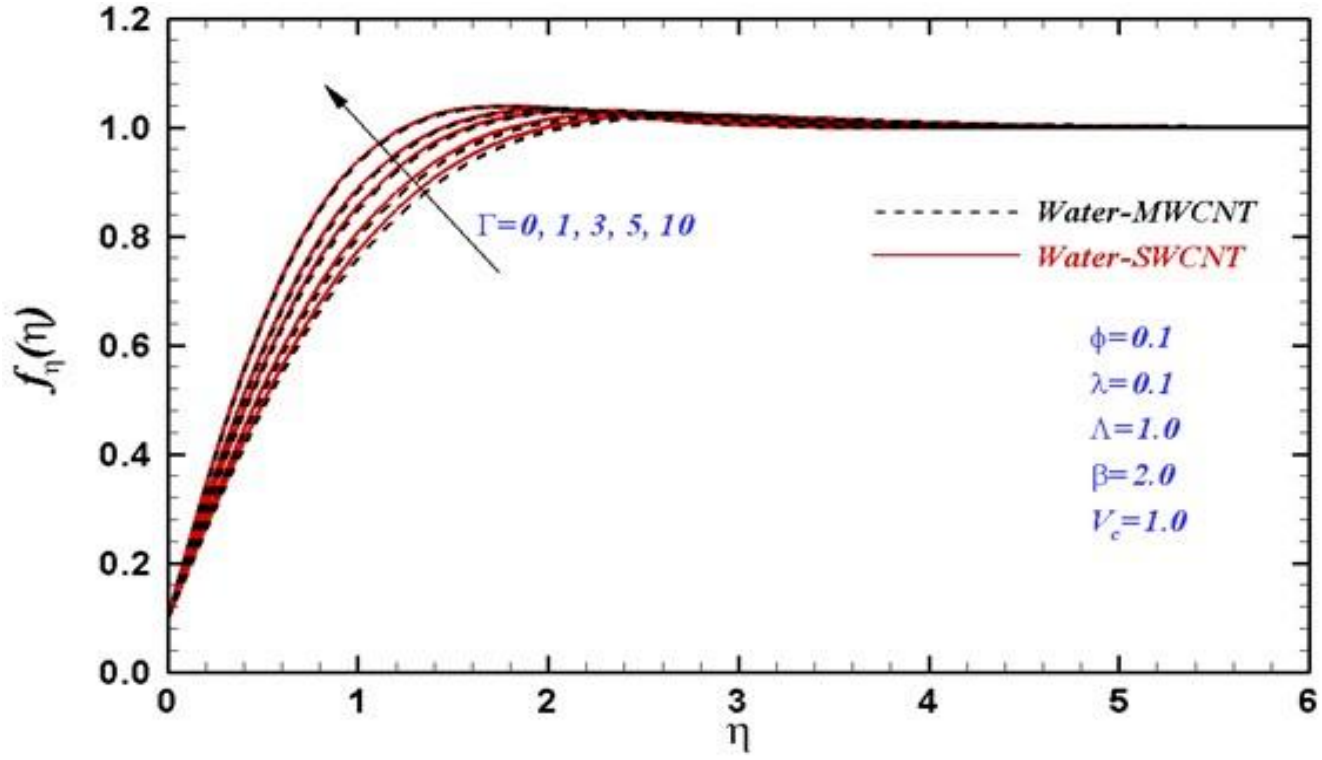


Fig 8. Influence of Γ on $f_\eta(\eta)$.

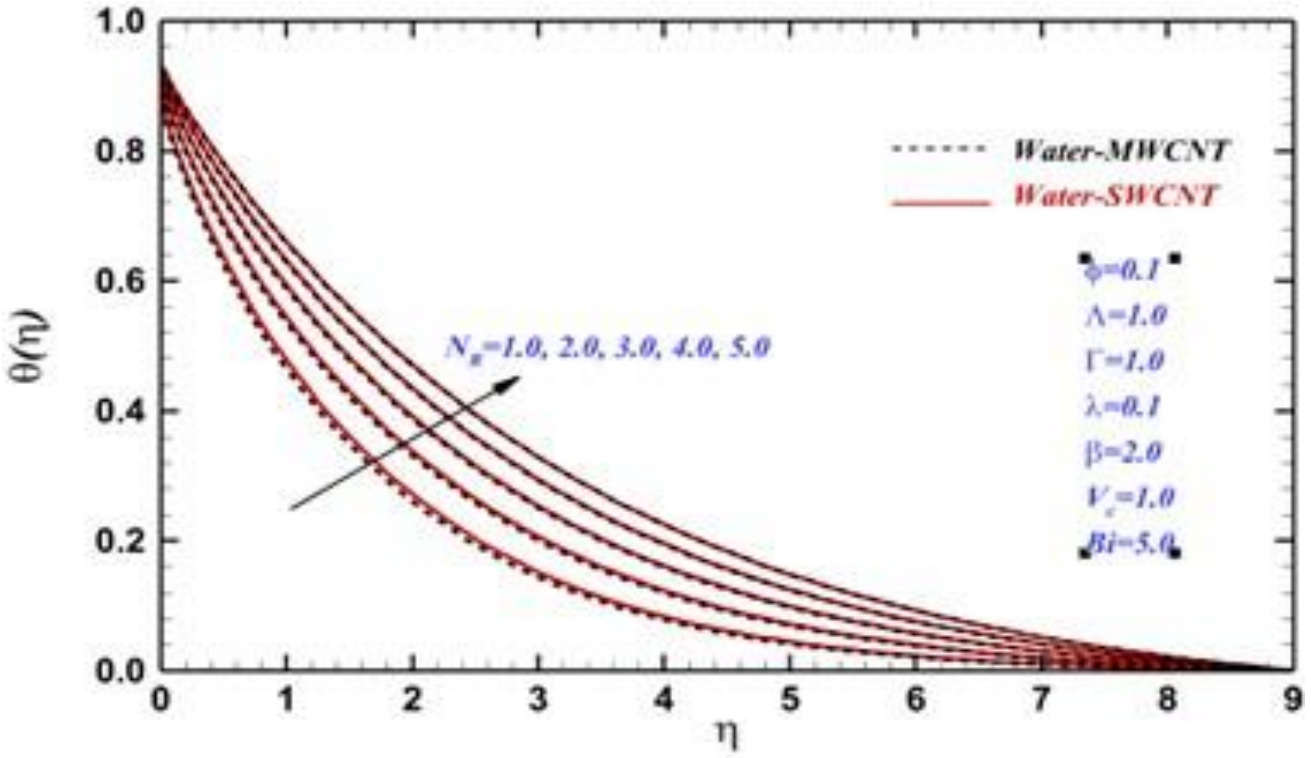


Fig 9. Influence of N_R on $\theta(\eta)$.

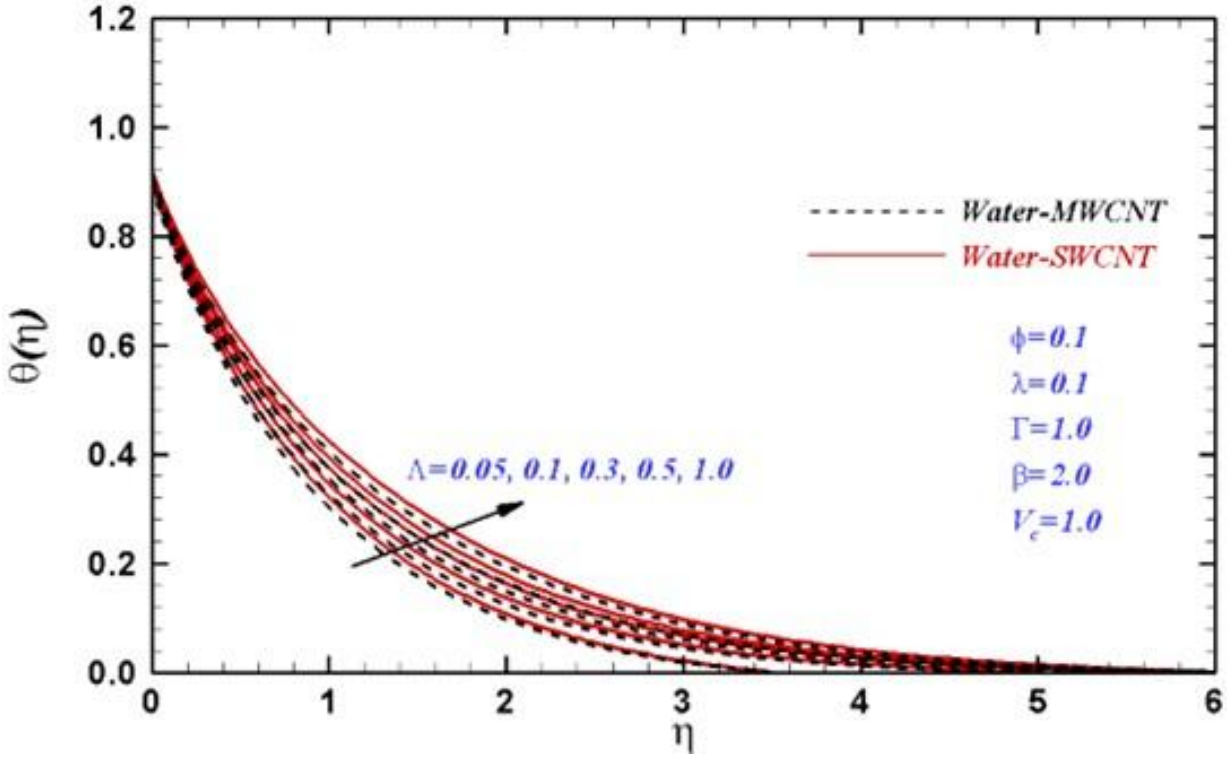


Fig 10. Effect of the Λ on $\theta(\eta)$.

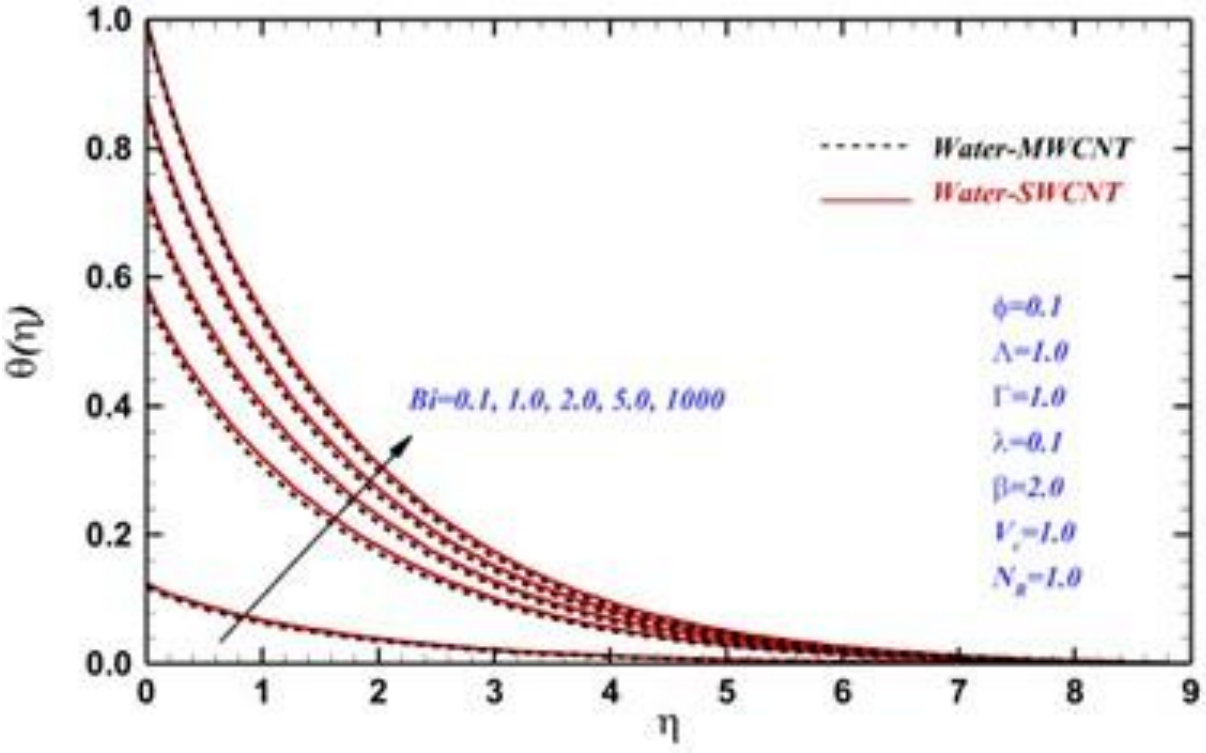


Fig 11. Effect of Bi on $\theta(\eta)$.

Fig 7 denotes the effect of V_C on the $f_\eta(\eta)$. The $f_\eta(\eta)$ Profile decreases for increasing values of V_C. From a physical point of view, when V_C Rises in the form of suction, more fluid is pulled to the surface, suppressing fluid motion and decreasing velocity in the boundary layer. This fluid loss lowers the velocity profile and shows down momentum transmission. Higher suction inhibits flow separation, thickens the boundary layer of momentum, and physically stabilizes the flow.

Fig 8 represents the impact of the porosity parameter on the velocity profile $f_\eta(\eta)$. As the parameter Γ is raised, the $f_\eta(\eta)$ increases. Physically, permeability of the porous material increases as the porosity is enhanced. This decreases flow resistance, causing velocity to increase within the boundary layer. Physically, increasing porosity promotes fluid motion and momentum transmission across the porous structure.

Fig.9 represents the impact of N_R on the temperature profile $\theta(\eta)$. The temperature profile increases with increasing N_R parameter. Physical point of view, increased thermal radiation slows the pace at which heat escapes from the surface and into the surroundings, thickening the thermal boundary layer and raising fluid temperature. In high-temperature applications, including combustion, solar collectors, space re-entry flows, and nanofluid heating systems, this behaviour is crucial.

Fig. 10 represents the impact of the couple stress constraint. Λ on temperature profile $\theta(\eta)$. The temperature profile increases with increasing. Λ Constraint. Physically, increased couple stress reduces convective heat removal and encourages thermal storage in the fluid, resulting in a thicker thermal boundary layer and a higher overall fluid temperature. Heat dispersion is influenced by microstructural rotations in microfluidic devices, lubricants, polymeric fluids, and biological suspensions.

Fig. 11 represents the influence of the Boit number. Bi on temperature profile $\theta(\eta)$. The temperature profile increases with enhancing the Bi. Heat is transported from the surrounding fluid more effectively when the Bi Rises because surface convection becomes greater. Physically, it means the solid surface and fluid have a greater thermal contact and better heat transfer capability.

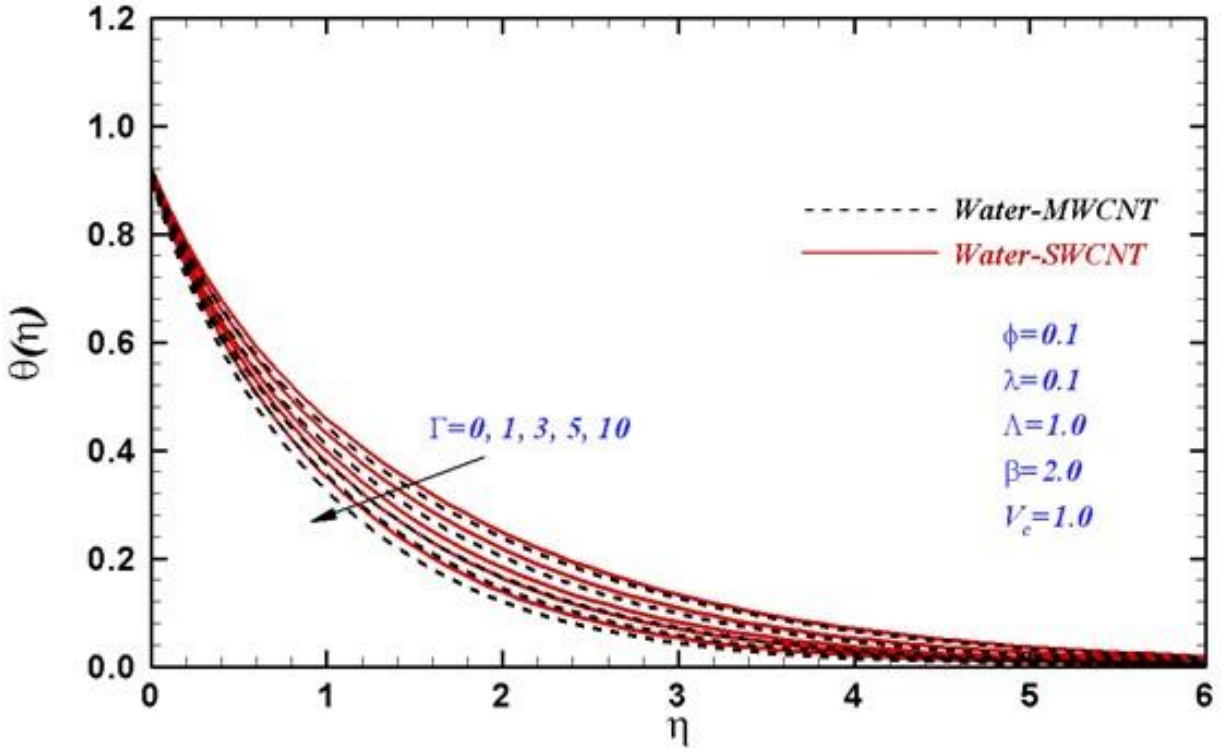


Fig 12. Effect of Γ on $\theta(\eta)$.

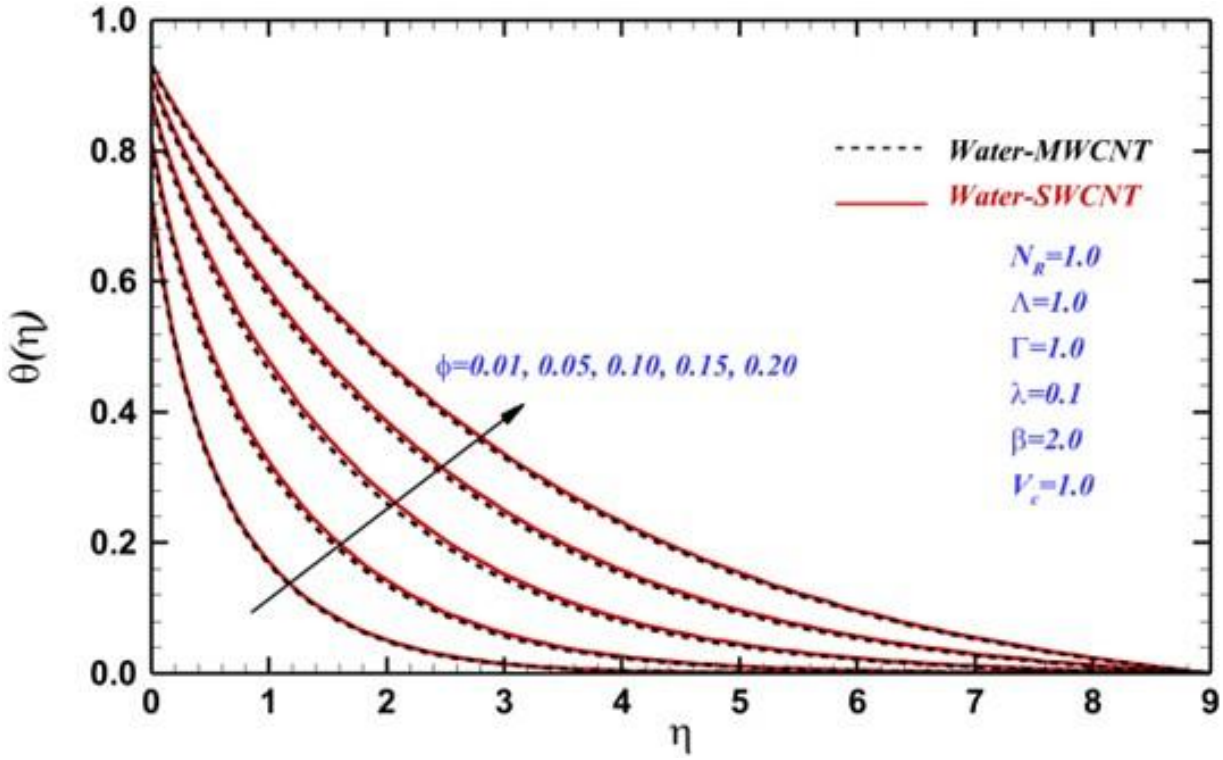


Fig 13. Effect solid volume fraction ϕ on $\theta(\eta)$.

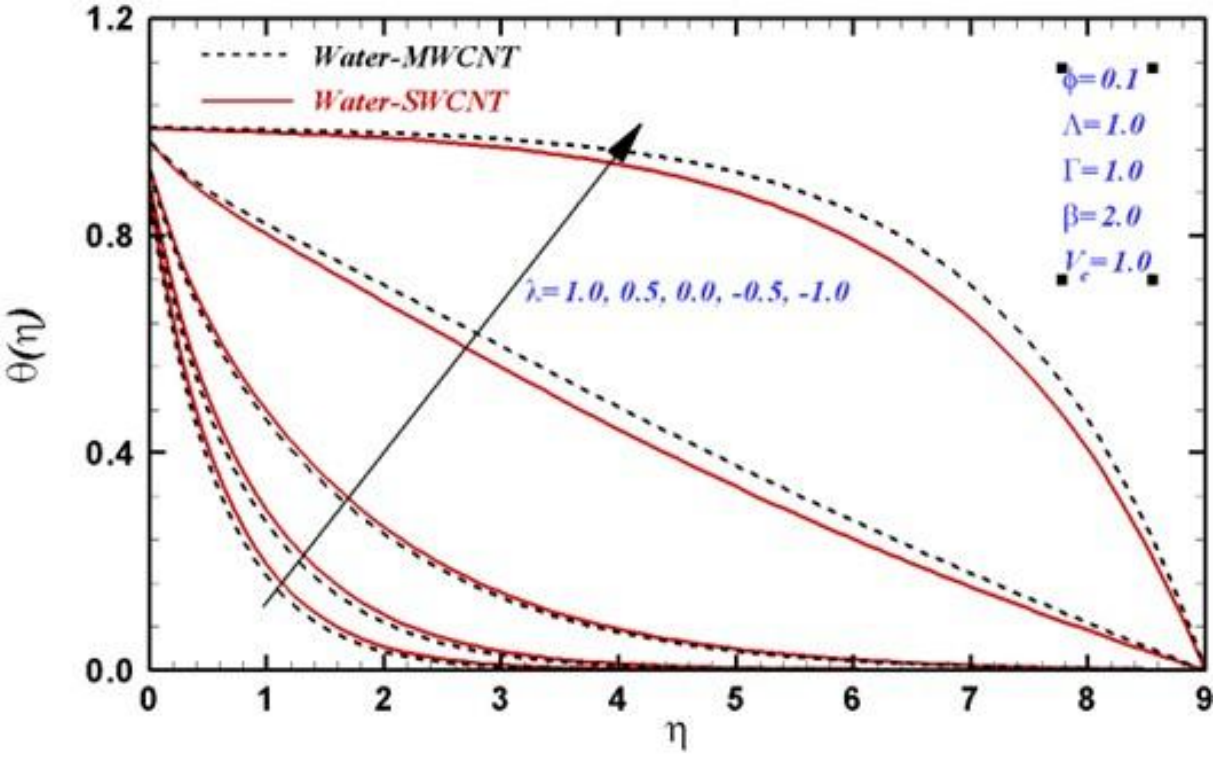


Fig 14. Impact of Shrinking/stretching λ on $\theta(\eta)$.

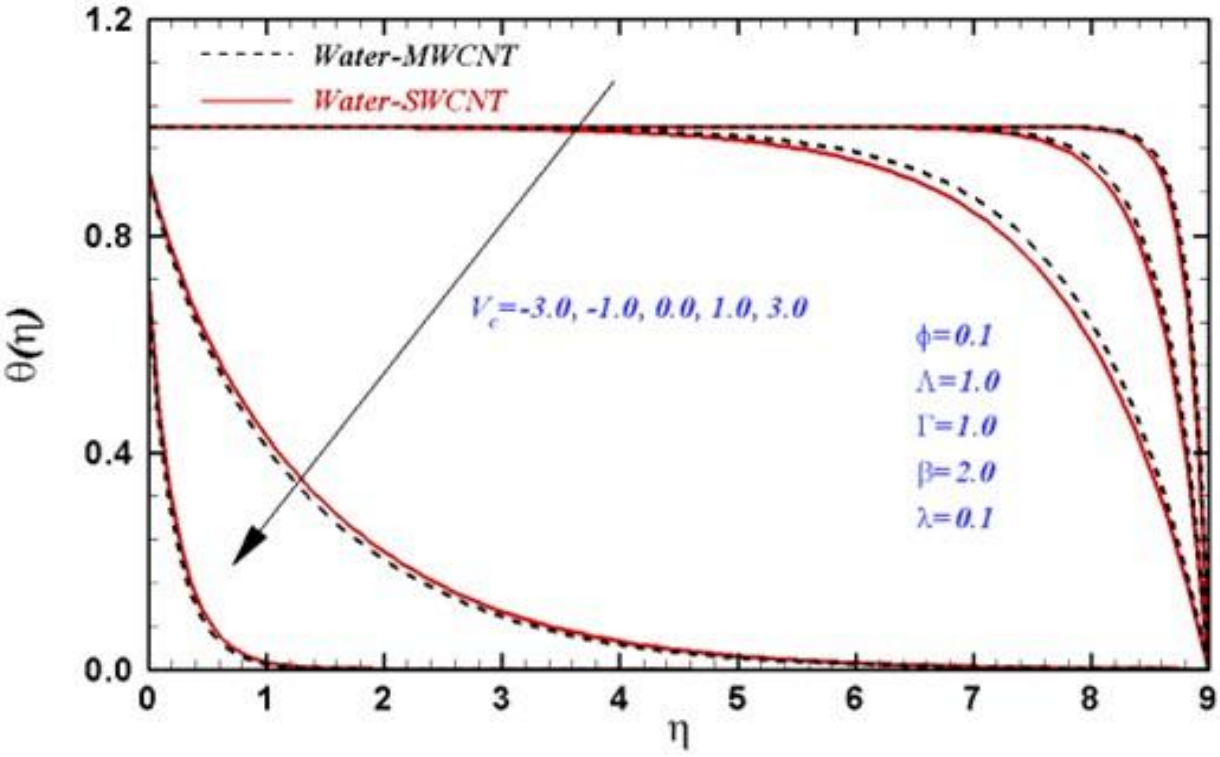


Fig 15. Effect of mass transpiration V_C on temperature profile $\theta(\eta)$.

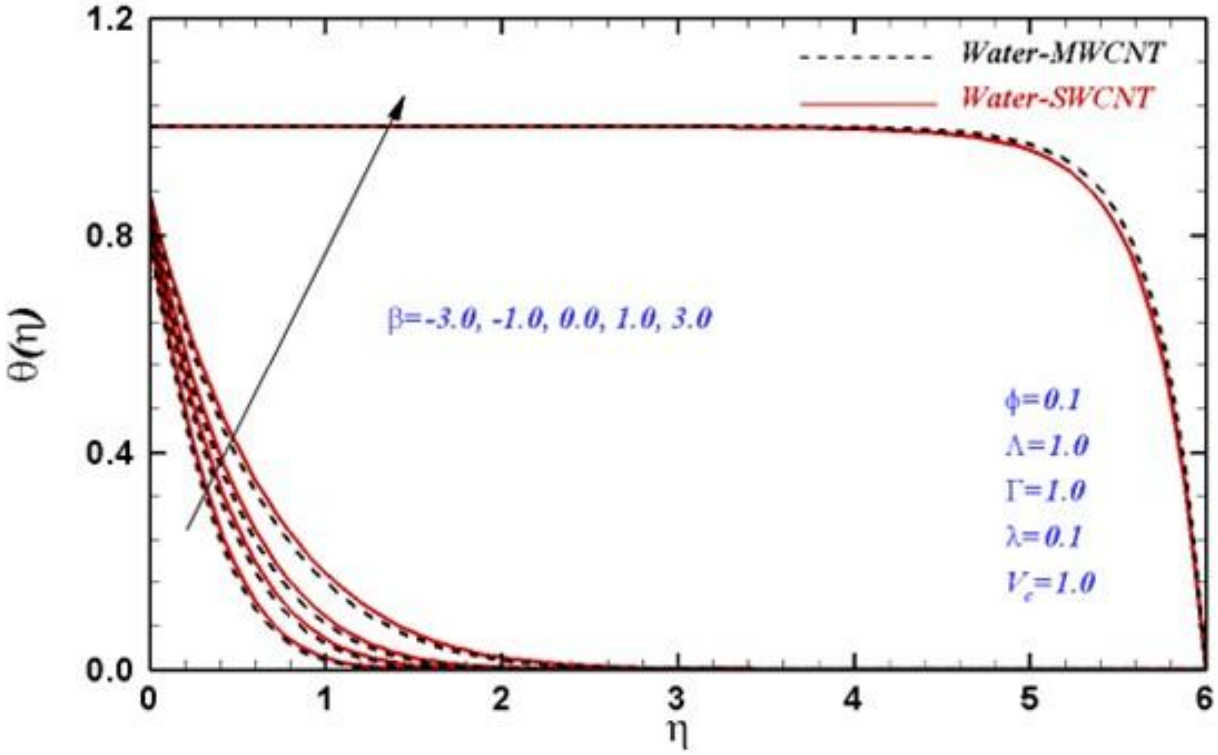


Fig 16. Impact of the unsteadiness parameter β on $\theta(\eta)$.

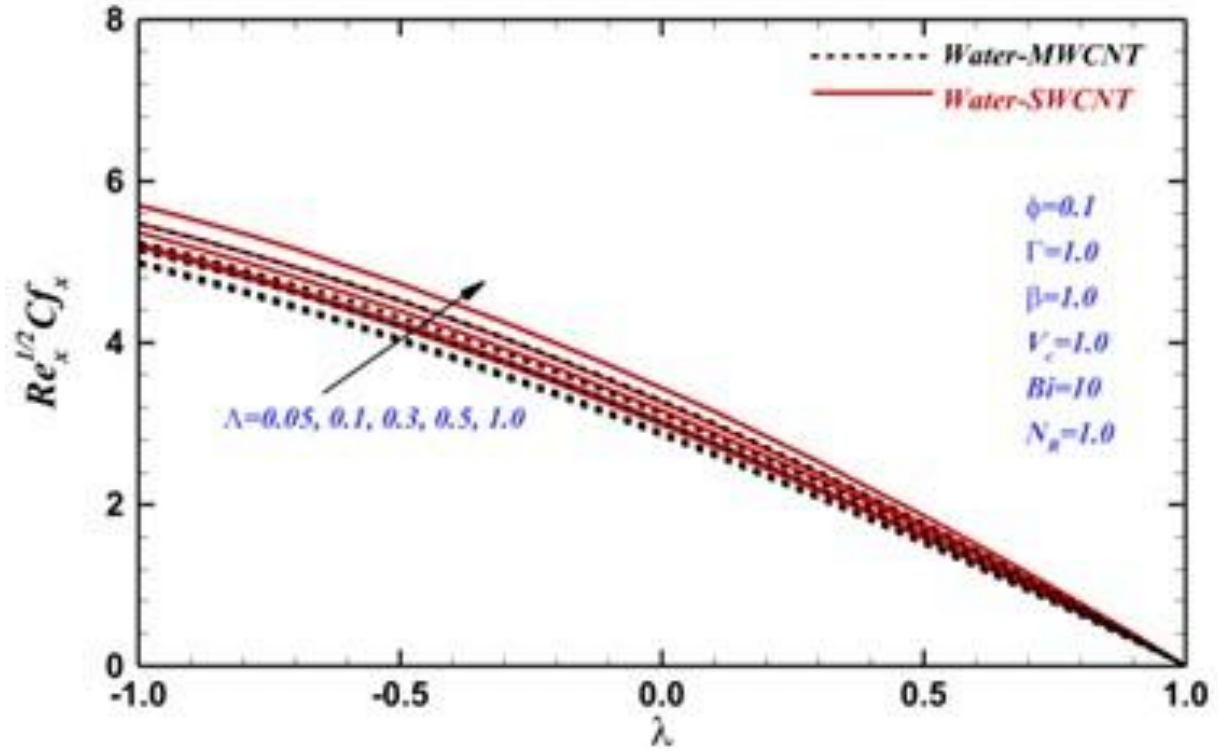


Fig 17a. Effect of Couple stress parameter Λ on Cf_x.

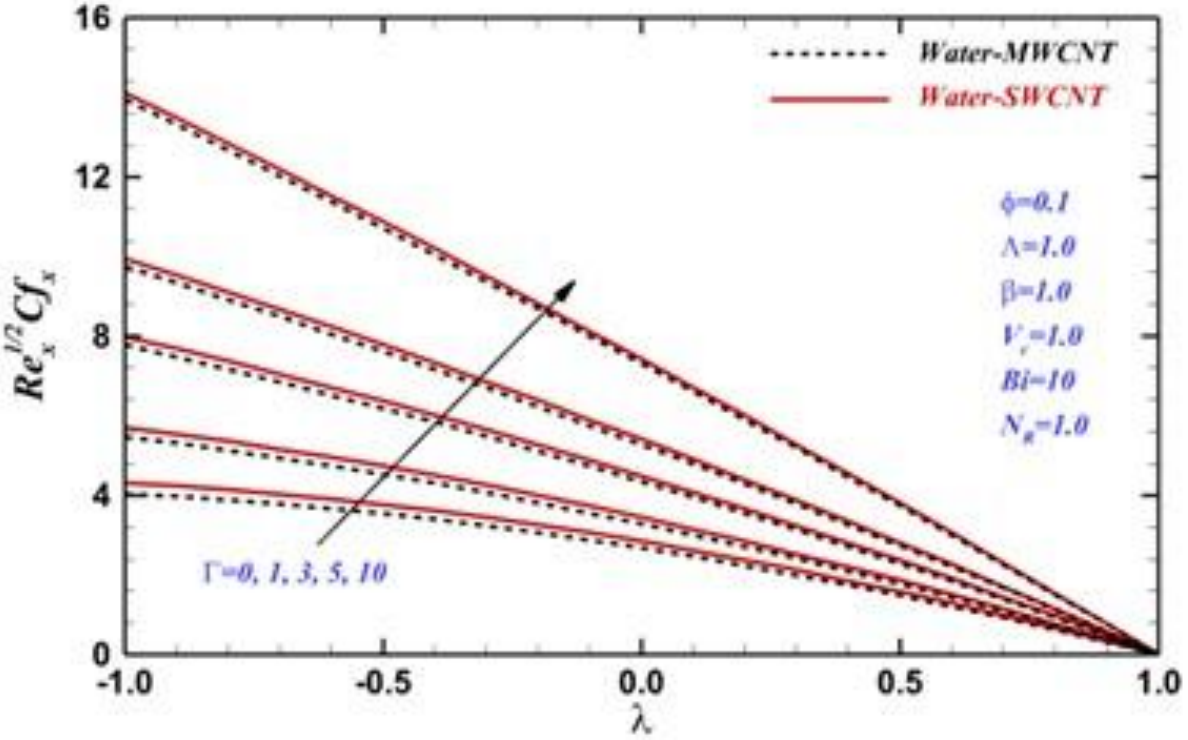


Fig 17b. Effect of porosity parameter Γ on Cf_x.

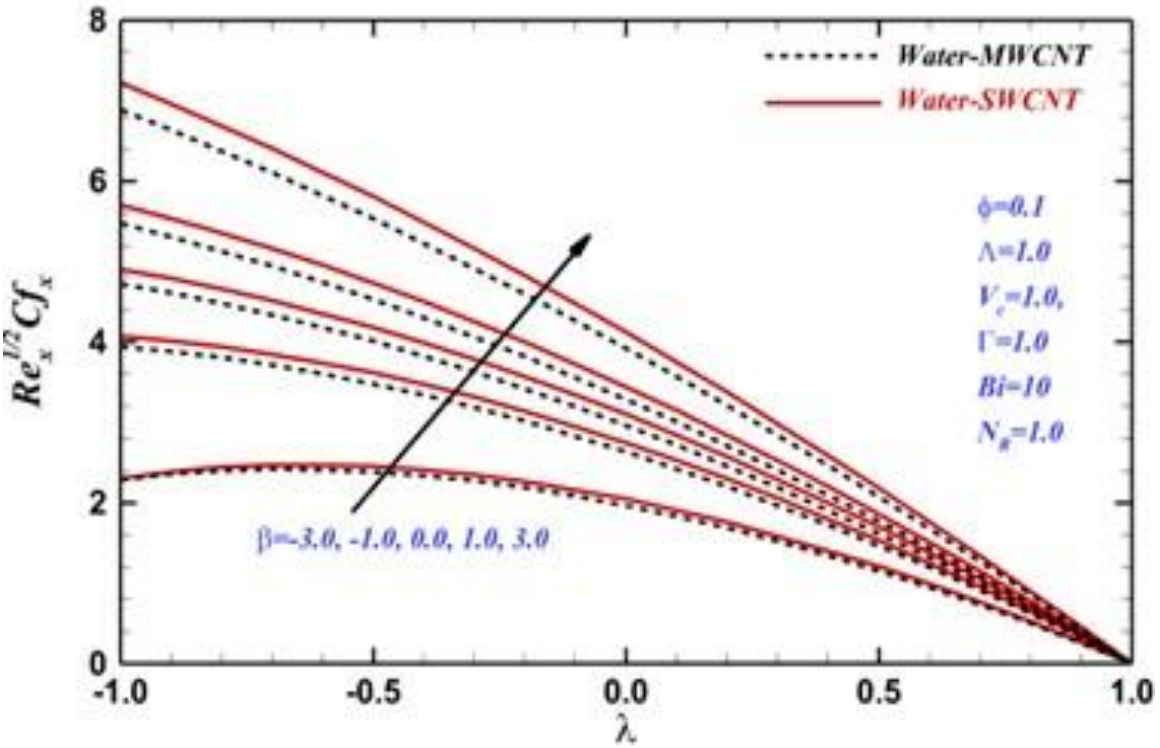


Fig 17c. Effect of unsteadiness parameter β on Cf_x.

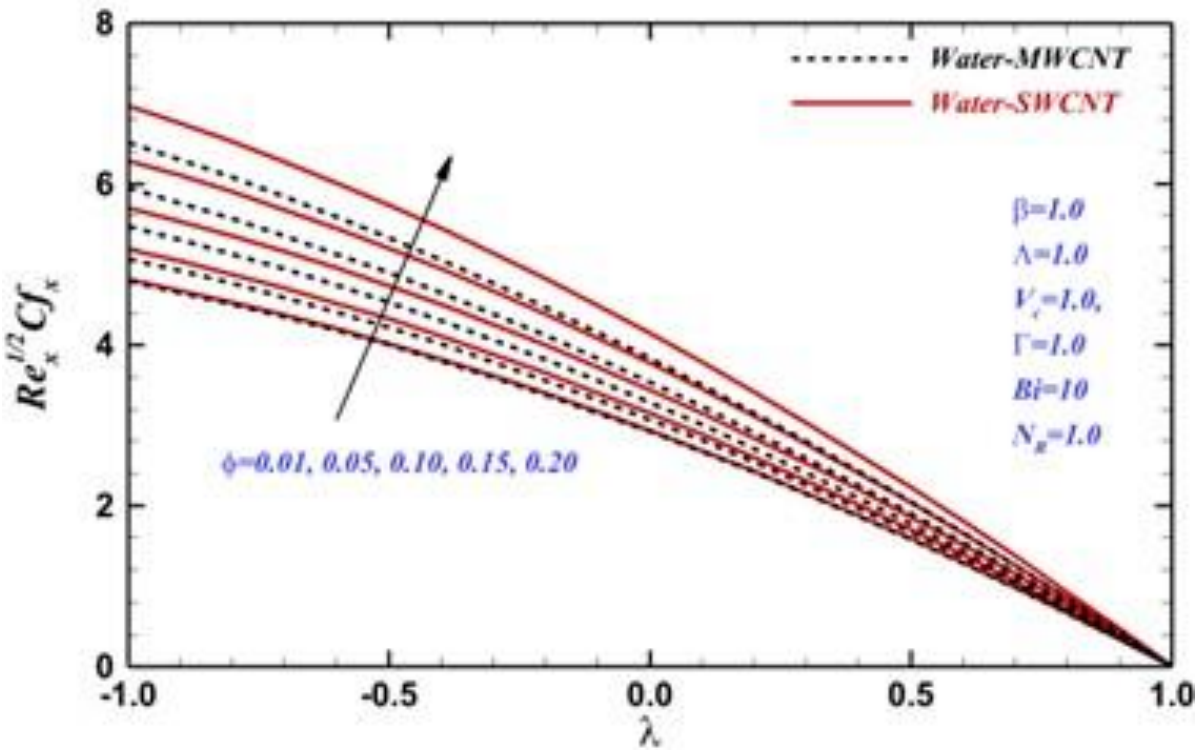


Fig 17d. Effect of solid volume fraction ϕ on Cf_x.

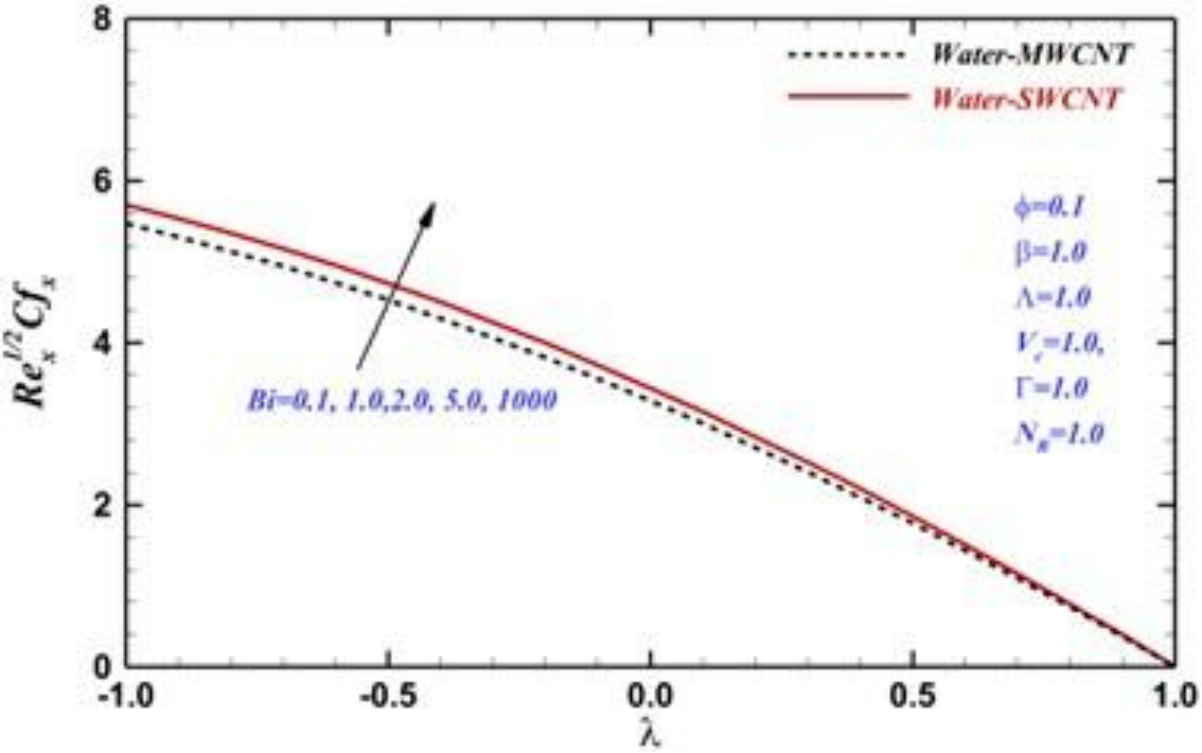


Fig 17e. Effect of Biot number Bi on Cf_x.

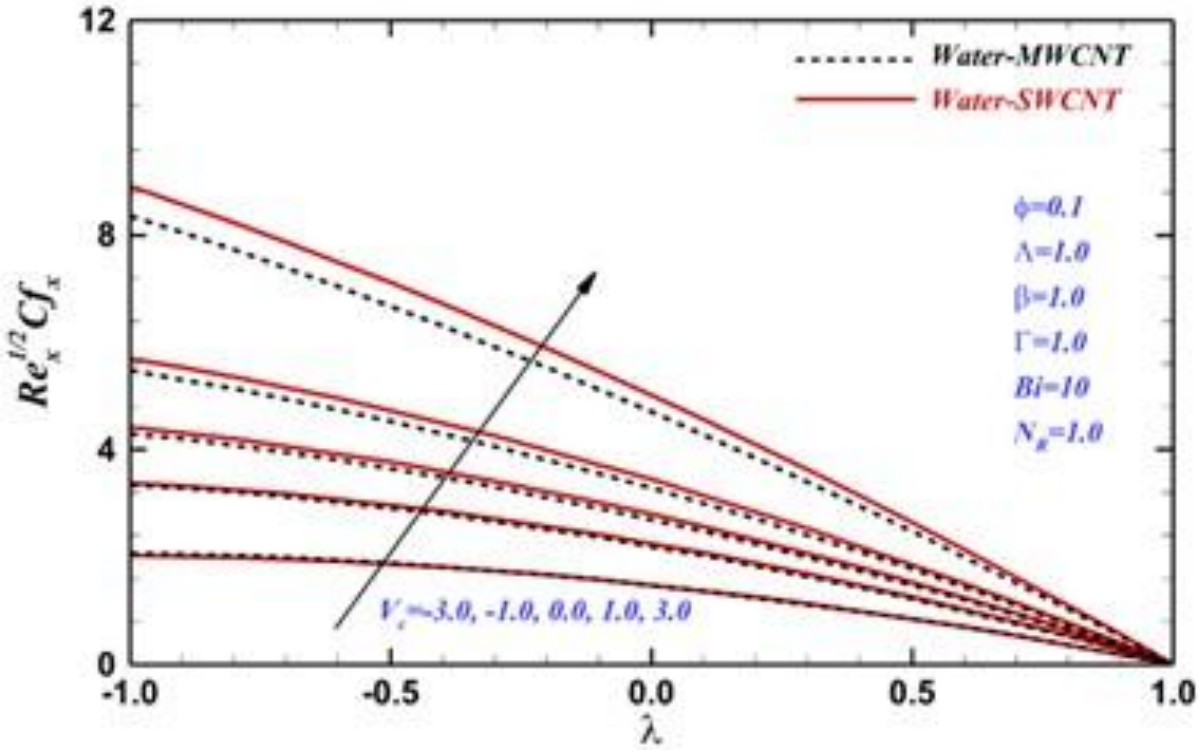


Fig 17f. Effect of mass transpiration V_C On.

Fig.12 represents the effect of the porosity parameter. Γ On the temperature profile. Enhancing the Γ Parameter decreases the $\theta(\eta)$ Profile. Γ Parameter increases, the medium becomes more permeable, allowing fluid to flow more radially through the porous structure. This improves convective heat transmission, resulting in a warmer temperature profile in the boundary layer. Higher porosity enhances the physical efficiency of heat transmission in packed-bed reactors, geothermal systems, filters, and porous channels. It demonstrates how heat and fluid may enter porous materials more deeply when there is a greater area.

Fig. 13 indicates the impact of the solid volume fraction. ϕ on temperature profile $\theta(\eta)$. Enhancing the ϕ Parameter increases the $\theta(\eta)$. Physically, the solid volume percentage increases, and more nanoparticles are suspended in the base fluid, increasing the mixture's total thermal conductivity. The temperature profile rises, and the fluid retains more heat close to the surface as a result of this enhanced heat-carrying capacity. In nanofluids used for cooling, lubrication, and industrial heat exchange systems, a higher solid volume fraction physically denotes stronger thermal diffusion, better energy transport, and enhanced heat transfer performance.

Fig. 14 represents the impact of the stretching/shrinking parameter λ on temperature profile $\theta(\eta)$. The temperature profile increases with a decrease in λ Parameter. The sheet flows more

slowly or compresses the fluid as the λ Parameter drops, which lessen convective heat transfer away from the surface. This reduces heat loss and forms a thicker thermal barrier layer, resulting in a higher temperature profile. Physically, it means that the fluid's thermal diffusion is decreased, heat retention is stronger close to the wall, and cooling effectiveness is decreased. Enhancing the V_C decreases the $\theta(\eta)$ Profile. The sheet flows more slowly or compresses the fluid as the stretching/shrinking parameter drops, which lessens convective heat transfer away from the surface. This reduces heat loss and forms a thicker thermal barrier layer, resulting in a higher temperature profile. Physically, it means that the fluid's thermal diffusion is decreased, heat retention is stronger to the wall, and cooling effectiveness is decreased.

Fig.16 represents the effect of the β on temperature profile $\theta(\eta)$. The temperature profile rises with growing values of β. The parameter rises, the flow becomes more time-dependent, and the fluid reacts more slowly to the temperature changes, limiting heat diffusion away from the surface. As a result, the temperature profile rises and the thermal boundary layer becomes thicker. Physically, more unsteadiness means less cooling, more heat retention near the surface, and delayed thermal relaxation in the fluid.

Fig.17a-Fig.17f represents the impact of different parameters, like the couple stress parameter (Λ), porosity parameter (Γ), unsteadiness (β), parameter volume fraction (ϕ), Biot number (Bi), mass transportation (V_C), on skin friction coefficient (Cf_x). Skin friction coefficient increases with increasing all parameters. Increasing the couple stress parameter increases the micro-rotational viscosity, thickening the near-wall area and increasing shear resistance. Higher porosity enhances fluid penetration and momentum exchange inside the porous medium, hence increasing wall drag. Increasing unsteadiness reduces fluid adjustment to surface motion, which increases shear stress. The fluid becomes mechanically and thermally thicker with a greater solid volume percentage, increasing friction near the wall. A higher Biot number increases heat exchange at the surface, creating thermal gradients and thereby strengthening viscous forces. Lastly, increasing mass transpiration through suction causes fluid to be drawn towards the surface, which increases skin friction and compresses the boundary layer. Physically, all of these effects represent increased fluid-wall contact, higher momentum transfer, and more resistance to motion at the boundary.

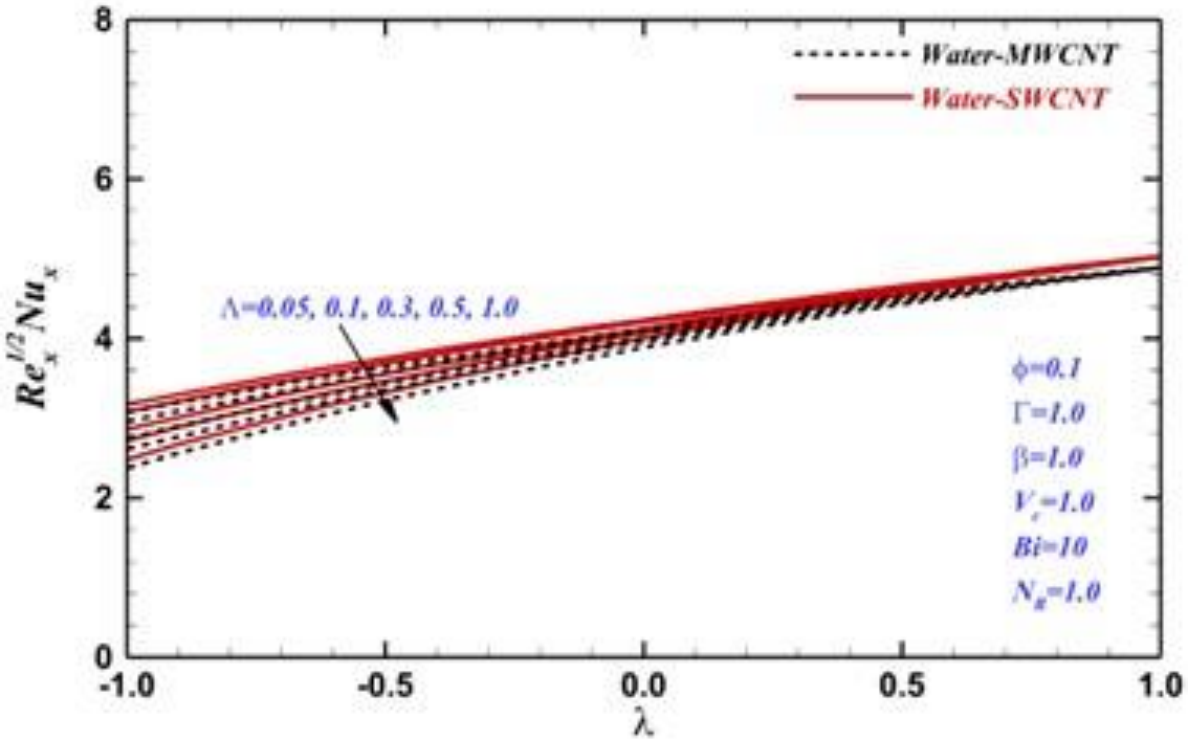


Fig 18a. Effect of the Couple stress parameter Λ on Nu_x.

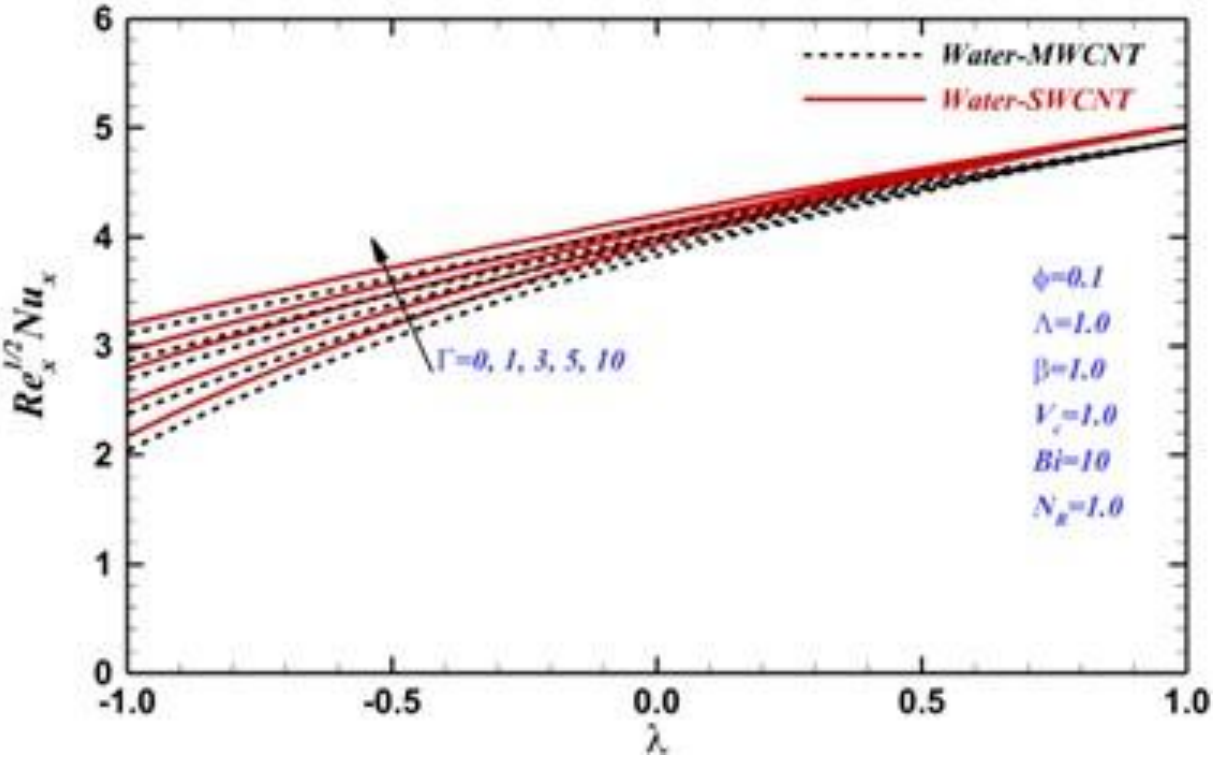


Fig 18b. Effect of porosity parameter Γ on Nu_x.

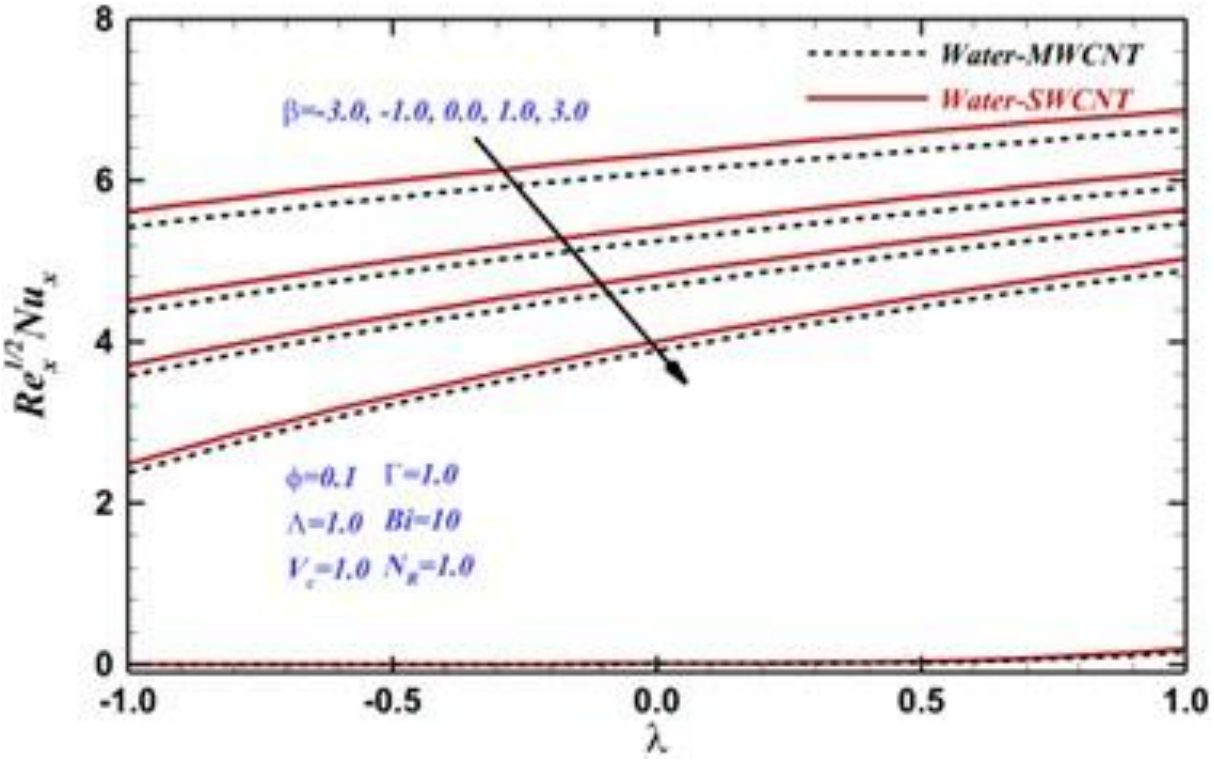


Fig 18c. Effect of unsteady parameter β on Nu_x.

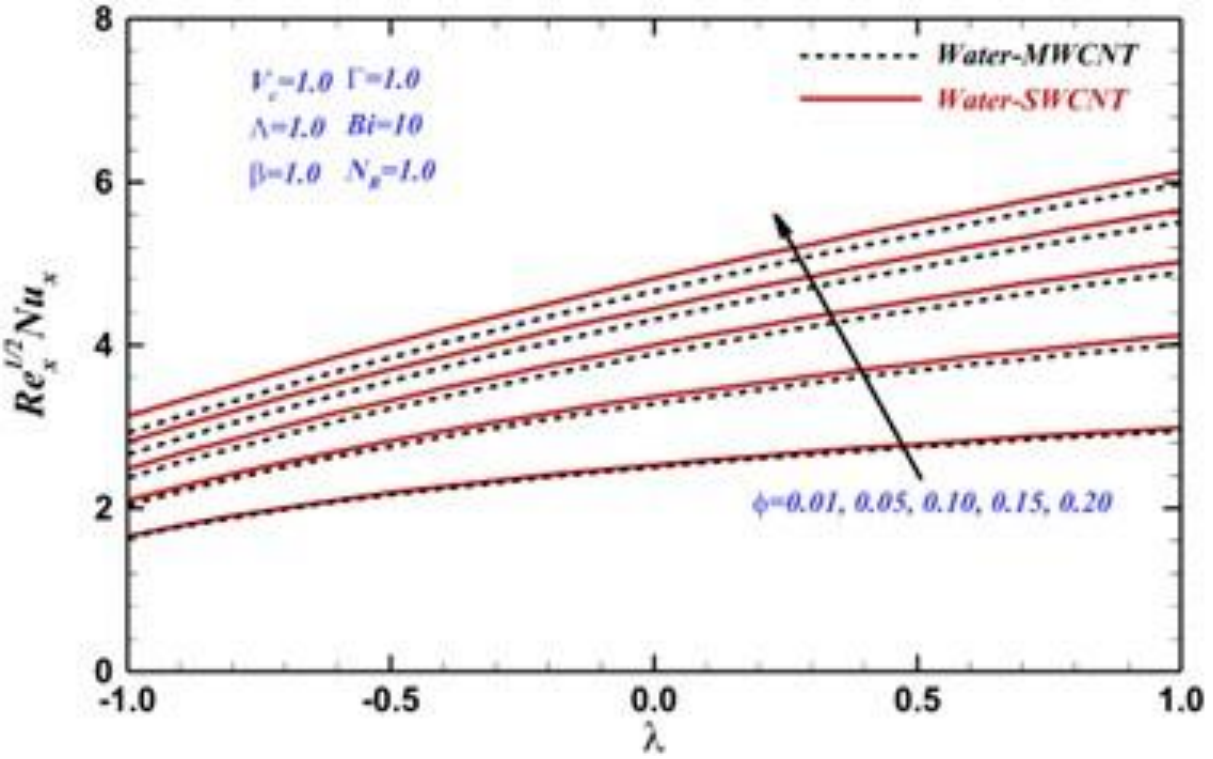


Fig 18d. Effect of the solid volume fraction parameter ϕ on Nu_x.

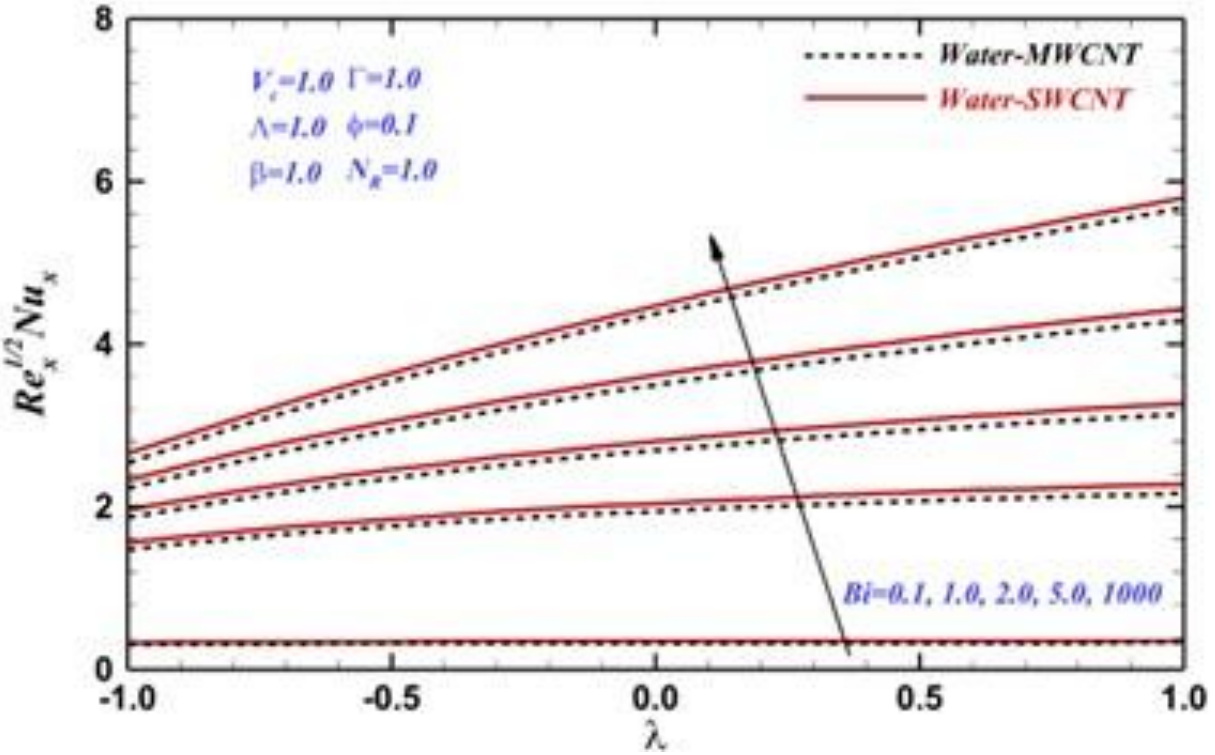


Fig 18e. Effect of Biot number Bi on Nu_x.

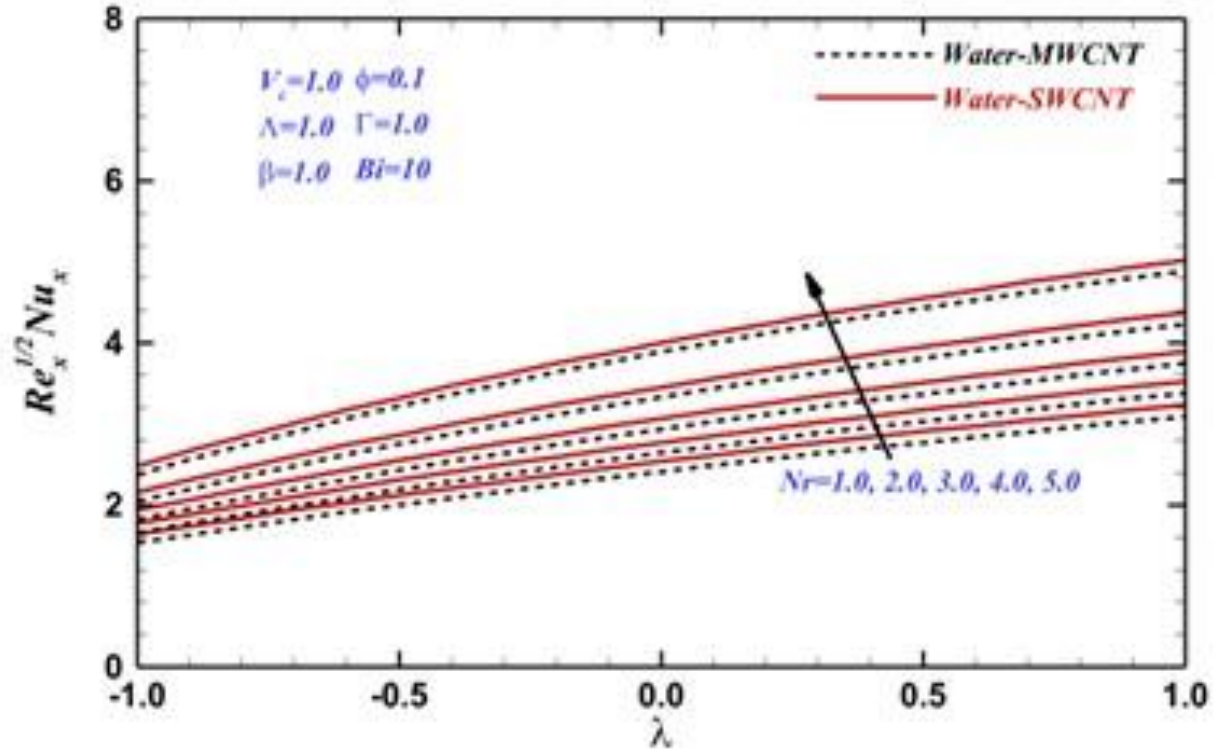


Fig 18f. Effect of Thermal radiation parameter Nr on Nu_x.

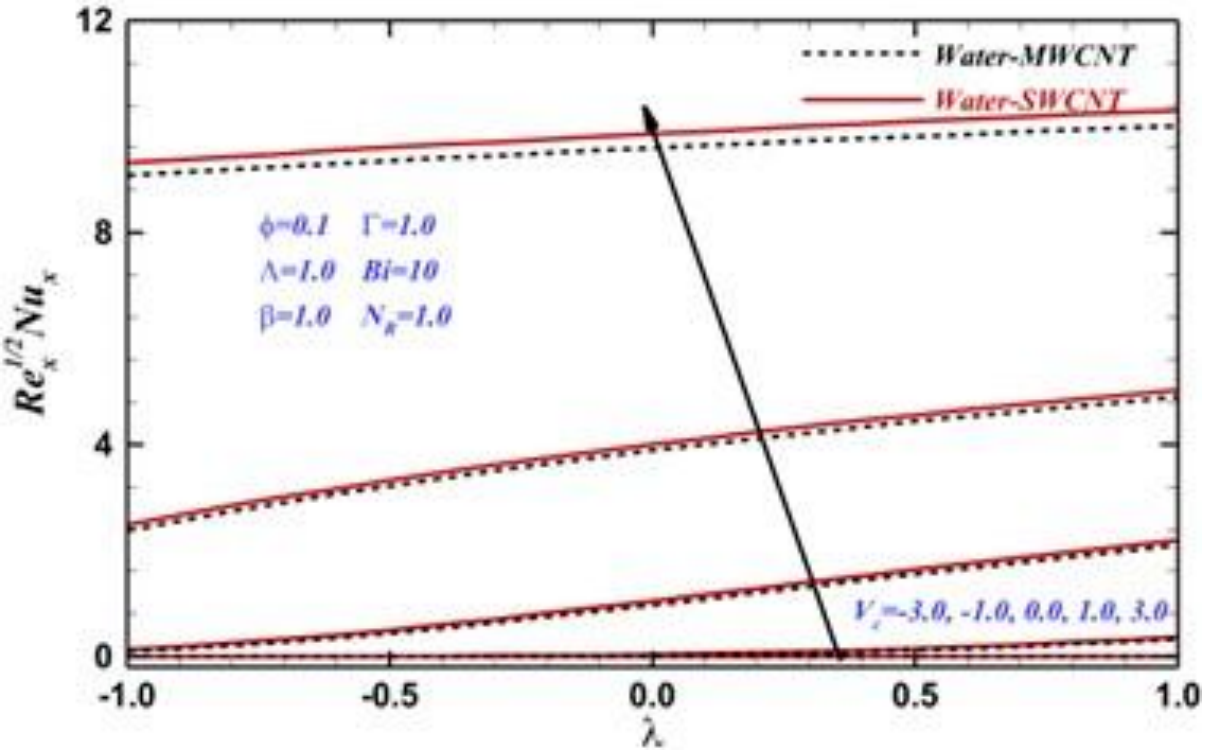


Fig. 18g. Effect of mass transpiration parameter V_C on Nu_x.

Fig 18a-Fig 18g represents the impact of different parameters, like the couple stress parameter (Λ), porosity parameter(Γ), unsteadiness parameter (β), volume fraction (ϕ), Biot number (Bi), Thermal radiation parameter (Nr), mass transportation (V_C), on Nusselt number coefficient (Nu_x). Enhancing the Λ Parameter decreases the Nu_x Number. Physically, the Couple stress fluid has higher heat diffusion due to the increased rotating motion of fluid particles. Increases the Γ Parameter increases the Nu_x. Physically, it improves mixing and energy exchange inside the porous structure, resulting in increased heat transfer rates. Enhancing the β Parameter decreases the Nu_x. Physically, time-dependent stretching increases the efficiency of heat removal. Increasing the ϕ Parameter increases the Nu_x Number. From a physical point of view, nanofluids carry more energy, resulting in higher convective heat transfer. Enhancing the Bi The number increases the Nu_x Number. Physically, this suggests a greater thermal contact between the solid surface and the fluid, which results in increased heat transfer efficiency. Increasing the Nr Parameter increases the Nu_x Number. This is because radiation accelerates energy loss from the surface and increases heat dissipation. Enhancing V_C Parameter increases the Nu_x Number. Physically, this helps to stabilize the thermal field and facilitates effective cooling.

Conclusion

The current work concentrates on the impacts of porous medium and radiation on unstable couple stress nanofluid flow over a stretching/shrinking surface. The nonlinear PDEs are converted into nonlinear ODEs with the help of a proper similarity approach, and then the solution is obtained using an analytical method. The analysis is carried out in two cases: water-SWCNT and water-MWCNT. The important points from the study are summarized as follows:

1. The axial velocity decreases for growing values of mass transpiration, couple stress, and stretching/shrinking parameter.
2. The temperature profile boosts for increasing values of the Couple stress, Biot number, porosity parameter, solid volume fraction, unsteadiness parameter, and stretching/shrinking parameter.
3. The temperature profile is found to drop for augmented values of mass transpiration.
4. The results show that Skin friction increases for the Couple stress parameter, porosity parameter, unsteadiness parameter, solid volume fraction, Biot number, and mass transpiration.
5. It is found that the Nusselt number decreases for the Couple stress parameter, unsteady parameter, but increases for mass transpiration parameter, radiation parameter, Biot number, solid volume fraction, and porosity parameter.

Author Contributions: U.S.M and K.N: supervision, methodology, investigation, assisted in writing and data extraction, supervision, and referencing; K.N and U.S.M methodology and analysis, investigation, writing original draft, language, and review-editing; U.S.M, O.M, B.B and S.N: result validation, proofreading, and review editing.

Data availability statement: All data generated or analysed during this study are included in this published article.

References

[1] Sakiadis BC. Boundary-layer behaviour on a continuous solid surface, boundary layer equation for two-dimensional and axisymmetric flow. AIChE J 1961; 7:26-8. http://dx.doi.org/10.1002/aic.690070108.

[2] Crane LJ. Flow past a stretching plate. Z Angew Math Mech 1970; 21:645-47. http://dx.doi.org/10.1007/BF01587695.

[3] Hayat T, Shafiq A, Alsaedi A, Awais M. MHD axisymmetric flow of third-grade fluid between stretching sheets with heat transfer. Comput. Fluids. 2013; 86:103-108. https://doi.org/10.1016/j.compfluid.2013.07.003.

[4] Mohanty D, Mahanta G, Shaw S. Thermal and irreversibility analysis on Cattaneo-Christov heat flux-based unsteady hybrid nanofluid flow over a spinning sphere with interfacial nanolayer mechanism. J. Therm Anal Calorim. 2023;148: 12269-12284. https://doi.org/10.1007/s10973-023-12464-y.

[5] Mahabaleshwar, U. S., Vishalakshi, A. B., & Andersson, H. I. (2022). Hybrid nanofluid flow past a stretching/shrinking sheet with thermal radiation and mass transpiration. Chinese Journal of Physics, 75, 152-168.

[6] Kumar NN, Sastry DRVSRK, Shaw S. Irreversibility analysis of an unsteady micropolar CNT-blood nanofluid flow through a squeezing channel with activation energy-application in drug delivery. Comput. Methods Programs Biomed. 2022; 226:107156. https://doi.org/10.1016/j.cmpb.2022.107156.

[7] Sahu SK, Shaw S, Thatoi DN, Azam M, Nayak MK. Darcy-Forchheimer flow behaviour and thermal inferences with SWCNT/MWCNT suspensions due to shrinking rotating disk. Waves Random Complex Media. 2022;2094496. https://doi.org/10.1080/17455030.2022.2094496.

[8] Iijima S. Helical microtubules of graphitic carbon. Nature. 1991; 354:56-8. http://dx.doi.org/10.1038/354056a0.

[9] Kumar, R., Kumar, R., Sheikholeslami, M., & Chamkha, A. J. (2019). Irreversibility analysis of the three-dimensional flow of carbon nanotubes due to nonlinear thermal radiation and quartic chemical reactions. Journal of Molecular Liquids, 274, 379-392.

[10] Mahabaleshwar US. External regulation of convection in a weak electrically conducting non-Newtonian liquid with g-jitter.

[11] Yedhiri, S. R., Palaparthi, K. K., Kodi, R., & Asmat, F. (2024). Unsteady MHD rotating mixed convective flow through an infinite vertical plate subject to Joule heating, thermal radiation, Hall current, radiation absorption. Journal of Thermal Analysis and Calorimetry, 149(16), 8813-8826.

[12] Eswaramoorthi, S., Nasir, S., Loganathan, K., Gupta, M. S., & Berrouk, A. (2025). Numerical simulation of rotating flow of CNT nanofluids with thermal radiation, ohmic heating, and autocatalytic chemical reactions. Alexandria Engineering Journal, 113, 535-550.

[13] Divya, A., Ramasekhar, G., Nagaraja, K. V., & Narasimhamurthy, S. K. (2025). Linear regression analysis of Williamson hybrid nanofluid flow with thermal radiation: Numerical simulation. International Journal of Thermofluids, 101343.

[14] Mahabaleshwar, U. S., Sarris, I. E., Hill, A. A., Lorenzini, G., & Pop, I. (2017). An MHD couple stress fluid due to a perforated sheet undergoing linear stretching with heat transfer. International Journal of heat and mass transfer, 105, 157-167.

[15] Khan, D., Kumam, P., Suttiarporn, P., & Srisurat, T. (2024). Fourier's and Fick's laws analysis of couple stress MHD sodium alginate based Casson tetra hybrid nanofluid along with porous medium and two parallel plates. South African Journal of Chemical Engineering, 47, 279-290.

[16] Rana, S., Tabassum, R., Mehmood, R., Tag-eldin, E. M., & Shah, R. (2024). Influence of Hall current & Lorentz force with nonlinear thermal radiation in an inclined slip flow of couple stress fluid over a Riga plate. Ain Shams Engineering Journal, 15(1), 102319.

[17] Kumar, B., & Jangili, S. (2025). Heat transfer analysis of electroosmotic flow of couple stress fluid through a rotating circular microchannel. International Journal of Thermal Sciences, 208, 109359.

[18] Kumar, P., & Nandkeolyar, R. (2025). A new mathematical model for the magnetohydrodynamic couple stress Casson fluid flow in a channel with stretching wall. Numerical Heat Transfer, Part A: Applications, 86(7), 2022-2039.

[19] Vinodkumar Reddy, M., Ajithkumar, M., Zafar, S. S. B., Faizan, M., Ali, F., & Lakshminarayana, P. (2024). Magnetohydrodynamic stagnation point flow of Williamson hybrid nanofluid via stretching sheet in a porous medium with heat source and chemical reaction. Proceedings of the institution of mechanical engineers, part E: Journal of Process Mechanical Engineering, 09544089241239583.

[20] Singh, S. P., Upreti, H., & Kumar, M. (2024). Stagnation point flow of hybrid nanofluid driven towards a sinusoidal-radius permeable circular cylinder. International Journal of Modelling and Simulation, 1-13.

[21] Karthik, G., & Kumar, P. V. (2024). EMHD stagnation point flow of dusty hybrid nanofluid over a permeable stretching sheet: Radiative solar applications. Case Studies in Thermal Engineering, 54, 104044.

[22] Awati, V. B., Goravar, A., & Kumar, M. (2024). Spectral and Haar wavelet collocation method for the solution of heat generation and viscous dissipation in micro-polar nanofluid for MHD stagnation point flow. Mathematics and Computers in Simulation, 215, 158-183.

[23] Malvandi A, Hedayati F, Ganji D.D, Slip effects on unsteady stagnation point flow of a nanofluid over a stretching sheet, Powder Technology, Volume 253,2014, Pages 377-384, ISSN 0032-5910,https://doi.org/10.1016/j.powtec.2013.11.049.

[24] Kumar M, Reddy GJ, Kumar NN, Bég OA. Application of differential transform method to unsteady free convective heat transfer of a couple stress fluid over a stretching sheet. Heat Transfer—Asian Res. 2019; 48: 582-600. https://doi.org/10.1002/htj.21396.

[25] Mukhopadhyay S. Effect of thermal radiation on unsteady mixed convection flow and heat transfer over a porous stretching surface in porous medium, International Journal of Heat and Mass Transfer, Volume 52, Issues 13–14, 2009, Pages 3261-3265, ISSN 0017-9310, https://doi.org/10.1016/j.ijheatmasstransfer.2008.12.029.

[26] Vishalakshi, A.B.; Mahabaleshwar, U.S.; Sarris, I.E. An MHD Fluid Flow over a Porous Stretching/Shrinking Sheet with Slips and Mass Transpiration. Micromachines 2022, 13, 116. https://doi.org/10.3390/mi13010116.

[27] Shehzad S. A, Waqas M, Alsaedi A. and Hayat T, "Flow and Heat Transfer over an Unsteady Stretching Sheet in a Micropolar Fluid with Convective Boundary Condition," J. Appl. Fluid Mech., vol. 9, no. 3, pp. 1437–1445, 2016, doi: 10.18869/acadpub.jafm.68.228.24172.